DOI: 10.1002/chem.200800876

# Bonding and Bending in Zirconium(IV) and Hafnium(IV) Hydrazides

**Heike Herrmann, Julio Lloret Fillol, Thorsten Gehrmann, Markus Enders, Hubert Wadepohl, and Lutz H. Gade*[a]**

**Abstract:** Reaction of the dichloro complexes $[M(N_2^{TBS}N_{py})Cl_2]$ (M = Zr: **1**, Hf: **2**; TBS: *t*BuMe$_2$Si; py: pyridine) with one molar equivalent of $LiNHNPh_2$ gave mixtures of the two diastereomeric chlorohydrazido(1−) complexes $[M(N_2^{TBS}N_{py})(NHNPh_2)Cl]$ (M = Zr: **3a**,**b**, Hf: **4a**,**b**) in which the diphenylhydrazido(1−) ligand adopts a bent $\kappa^1$ coordination. This mixture of isomers could be cleanly converted into the deep green diphenylhydrazido(2−) complexes $[Zr(N_2^{TBS}N_{py})(NNPh_2)(py)]$ (**5**) and $[Hf(N_2^{TBS}N_{py})(NNPh_2)(py)]$ (**6**), respectively, by dehydrohalogenation with lithium hexamethyldisilazide (LiHMDS) in the presence of one molar equivalent of pyridine. Both complexes contain a linearly coordinated hydrazinediide for which a DFT-based frontier orbital analysis established bonding through one σ and two π orbitals. A high polarity of the M=N bond was found, in accordance with the description of hydrazinediide(2−) acting as a six-electron donor ligand. The pyridine ligand in $[M(N_2^{TBS}N_{py})(NNPh_2)(py)]$ (M = Zr: **5**, Hf: **6**) is substitutionally labile as established by line-shape analysis of the dynamic spectra ($\Delta G^{\neq} = 19$ kcal mol$^{-1}$). A change in denticity of the hydrazido unit from $\kappa^1$ to $\kappa^2$ was studied by DFT methods. Both forms are calculated to be very close in energy and are only separated by shallow activation barriers, which supports the notion of a rapid $\kappa^1$ to $\kappa^2$ interconversion. This process is believed to happen early on in the N−N scission in the presence of coupling reagents. Frontier orbital and natural population analyses suggest that a primarily charge-controlled nucleophilic attack at $N_\alpha$ is unlikely whereas interaction with an electrophile could play an important role. This hypothesis was tested by the reaction of **5** and **6** with one molar equivalent of $B(C_6F_5)_3$ to give $[Zr(N_2^{TBS}N_{py})(NNPh_2)\{B(C_6F_5)_3\}]$ (**7**) and $[Hf(N_2^{TBS}N_{py})(NNPh_2)\{B(C_6F_5)_3\}]$ (**8**). In these products, $B(C_6F_5)_3$ becomes attached to the $N_\alpha$ atom of the side-on bound hydrazinediide and there is an additional interaction of an *ortho*-F atom of a $C_6F_5$ ring with the metal centre.

**Keywords:** density functional calculations · hafnium · hydrazides · NMR spectroscopy · zirconium

## Introduction

The study of group 4 metal-catalysed reactions of hydrazines with unsaturated organic substrates has almost exclusively focussed on titanium.[1] The hydrohydrazination of alkynes,[2] its extension to a catalytic three-component iminohydrazination,[3] as well as its development into an efficient metal-catalysed indole synthesis are prominent examples.[4] Until very recently, there was only one example of a heavier group 4 hydrazido complex, $[Cp_2Zr(N_2Ph_2)(dmap)]$ (Cp: $C_5H_5$, dmap: 4-dimethylaminopyridine), which had been reported by Bergman and co-workers in 1991.[5] We have begun to extend this early work on zirconium hydrazides by using a tridentate diamidopyridyl ligand $[N_2^RN_{py}]^{2-}$ as a supporting ligand.[6] Originally developed by us to stabilise complexes containing reactive MN bonds and their derivatives,[7] this ligand platform has allowed the preparation and characterisation of $[Zr(N_2^{TBS}N_{py})(NNPh_2)(py)]$ (py: pyridine). A first study of its reactivity revealed exciting new patterns of reactivity based on N−N bond cleavage and N−E (E = main group element) bond formation.[8]

In these transformations the zirconium hydrazido complex $[Zr(N_2^{TBS}N_{py})(NNPh_2)(py)]$ formally reacts like a hypothetical nitrido/nitrene. It is assumed, however, that a free metallanitrene species is unlikely to play a role in the N−C and N−E coupling reactions observed by Bergman and us.[5,8] As an alternative reaction pathway, the direct attack of the

[a] Dr. H. Herrmann, Dr. J. L. Fillol, T. Gehrmann, Dr. M. Enders, Prof. Dr. H. Wadepohl, Prof. Dr. L. H. Gade
Anorganisch-Chemisches Institut
Universität Heidelberg
Im Neuenheimer Feld 270, 69120 Heidelberg (Germany)
Fax: (+49) 6221-545-609
E-mail: lutz.gade@uni-hd.de

  

donor/acceptor reagent at the $N_\alpha$ atom prior to N–N bond cleavage therefore needs to be considered.

As for the linear hydrazinediido ligand (**A**),[9] the high local charge at $N_\alpha$ and the unavailability of a suitable acceptor orbital primarily located on that atom has led us to consider alternative coordination modes of the hydrazide that would favour such an interaction. A bent $\kappa^2$ arrangement of the hydrazinediide (**B**) appeared to us to provide such an activated form and might thus act as a synthon for the metallanitrene-type reactive system.

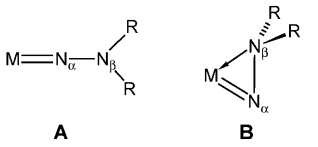


The accessibility and electronic properties of such bent group 4 metal hydrazides(2–), which have not been structurally characterised in mononuclear transition-metal complexes to date and which may also play a role in the N–N-cleavage/N–E-coupling reactions referred to above, is the object of this study. It was therefore of interest to model theoretically the bonding in linear and bent hydrazido species and to assess to what degree such a bent (side-on) hydrazide would possess donor/acceptor properties. Furthermore, a full account of the synthesis of the zirconium and, for the first time, hafnium hydrazinediides is given.

## Results and Discussion

**Synthesis and structural characterisation of zirconium and hafnium hydrazido(2–) complexes**: Reaction of the dichloro complexes $[M(N_2^{TBS}N_{py})Cl_2]$ (M = Zr: **1**, Hf: **2**) with one molar equivalent of $LiNHNPh_2$ gave mixtures of the two diastereomeric chlorohydrazido(1–) complexes $[M(N_2^{TBS}N_{py})(NHNPh_2)Cl]$ (M = Zr: **3a**,**b**, Hf: **4a**,**b**; Scheme 1). Whereas **3a** and **3b** were generated in a 75:25 ratio, the relative amounts of their hafnium congeners were 85:15. The infrared spectra of both **3a**,**b** and **4a**,**b** display intense bands at $\tilde{\nu} = 3218$ and 3230 $cm^{-1}$, respectively, which are due to the NH stretching vibration of the metal-coordinated hydrazido(1–) ligands.

The protons at the $N_\alpha$ atom of the hydrazido ligands resonate at $\delta = 6.54$ and 6.31 ppm for **3a** and **3b**, respectively ($\delta = 6.32$ and 6.18 ppm for **4a** and **4b**, respectively). The formation of the diastereomeric hydrazido(1–) complexes is also evident in the $^{15}N$ NMR spectra of the complexes. In the $^{15}N$-$^1H$ HMBC NMR spectrum of **3a**,**b**, displayed in Figure 1, the $^{15}N_\alpha$ signals of the hydrazide(1–) units are observed at $\delta = 203.6$ (**3a**) and 211.7 ppm (**3b**) as doublets ($^1J_{NH} = 63$ Hz) (the elliptically marked section in Figure 1), whereas the resonances of the $^{15}N_\beta$ nuclei are found at $\delta =$ 116.9 (**3a**) and 104.5 ppm (**3b**) ($NH_3$ used as external reference), as established by the coupling of the *ortho* protons of the two phenyl groups (represented by the rectangular box in Figure 1).

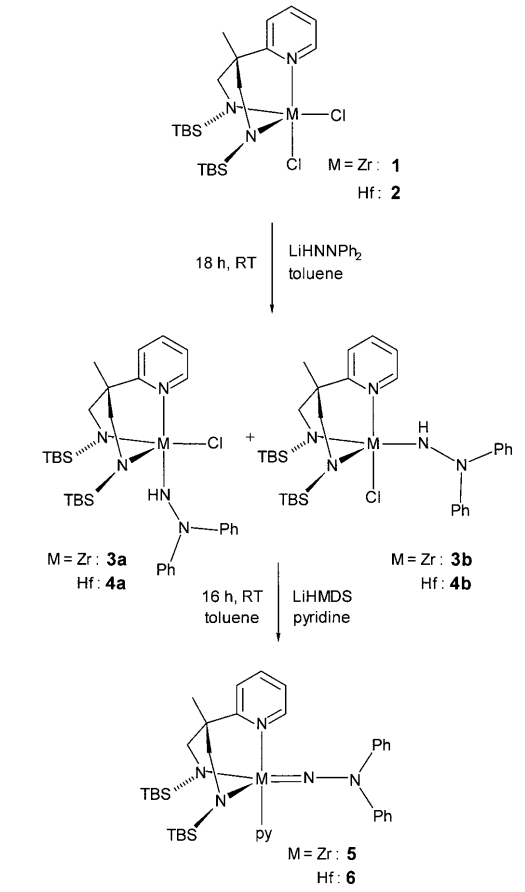


Scheme 1. Synthesis of the isomeric hydrazido(1–) complexes **3a** and **3b** as well as **4a** and **4b** and their conversion to the hydrazinediido(2–) zirconium complex **5** and the hydrazinediido(2–) hafnium complex **6**, respectively (TBS: $t$BuMe$_2$Si).

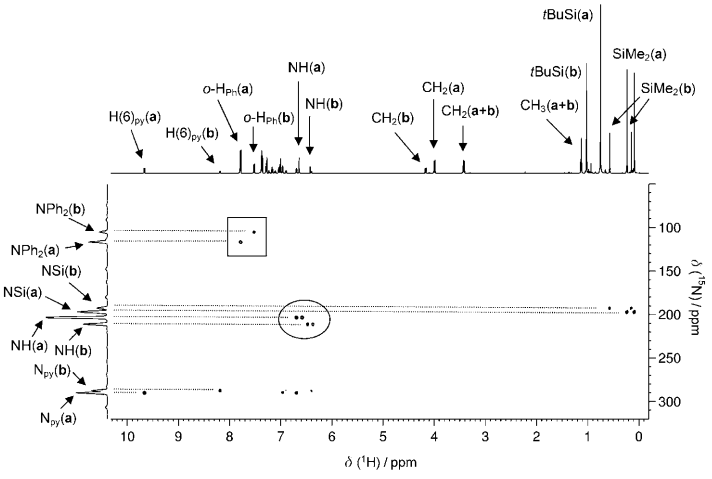


Figure 1. $^{15}N$-$^1H$ correlated NMR spectrum of **3a**,**b**. The $^{15}N_\alpha$ signals of the hydrazide(1–) units are observed at $\delta = 203.6$ (**3a**) and 211.7 ppm (**3b**) as doublets ($^1J_{NH} = 63$ Hz) (the elliptically marked section), whereas the resonances of the $^{15}N_\beta$ nuclei are found at $\delta = 116.9$ (**3a**) and 104.5 ppm (**3b**) (rectangular box).

  

Very similar data were obtained for the isomeric hafnium complexes **4a**,**b**. Furthermore, a $^1$H NOESY NMR spectroscopy study of **3a**,**b** is consistent with the structural assignment concerning the position of the hydrazido(1−) ligand in **3a** (axial as in **4a**) and in **3b** (equatorial as in **4b**).

These structural assignments were additionally confirmed by an X-ray diffraction study of the major component **3a**. Its molecular structure is displayed in Figure 2 along with

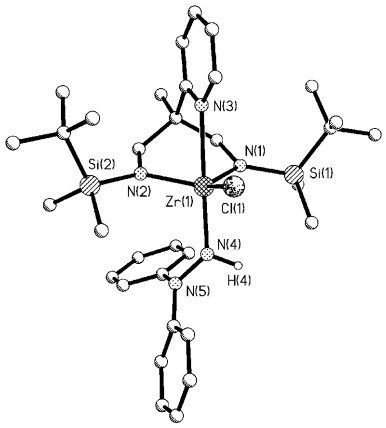


Figure 2. Molecular structure of complex **3a**. Selected bond lengths [Å] and angles [°]: Zr(1)–N(1) 2.037(6), Zr(1) –N(2) 2.018(5), Zr(1)–N(3) 2.437(6), Zr(1)–N(4) 2.080(6), N(4)–N(5) 1.427(8), Zr(1)–Cl(1) 2.467(2), N(4)–H(4) 1.0019; N(1)-Zr(1)-N(2) 106.4(2), N(1)-Zr(1)-N(3) 76.3(2), N(1)-Zr(1)-N(4) 100.8(2), N(2)-Zr(1)-N(3) 78.7(2), N(2)-Zr(1)-N(4) 101.8(2), N(3)-Zr(1)-N(4) 177.1(2), N(5)-N(4)-Zr(1) 130.5(4), N(4)-Zr(1)-Cl(1) 96.1(2).

the principal bond lengths and angles given in the legend. As already inferred from the NMR spectroscopy studies discussed above, the hydrazido(1−) unit occupies the axial coordination site *trans* to the pyridyl group of the tridentate ancillary ligand with a N(3)-Zr(1)-N(4) angle of 177.1(2)°, which is close to the idealised disposition of the two axial ligating atoms. The two amido functions of the tripod as well as the chloro ligand occupy the equatorial coordination sites (N(4)-Zr(1)-Cl(1) 96.1(2)°).

It is notable that the diphenylhydrazido ligand in **3a** is not bound to the metal centre through both of its nitrogen atoms as has been recently found for the closely related complexes [Zr($N_2^{TBS}N_{py}$)(NHNMe$_2$)Cl] and [Zr($N_2^{TBS}N_{py}$)-(NHNMePh)Cl];[10] the Zr(1)–N(5) distance in **3a** of 3.196 Å is well outside the range of bonding interactions. Probably due to the greater steric demand of the two phenyl substituents and the reduced Lewis basicity of the bis($N_\beta$-arylated) hydrazido unit in **3a** (as compared with HNNMe$_2$ and HNNMePh), a bent $\kappa^1$ coordination is observed in this case (Zr(1)-N(4)-N(5) 130.5(4)°). This is a rare structural motif, the only comparable molecular structures being those of [Ru(ttp)(NHNPh$_2$)$_2$][11] (ttp: tetrakis(*p*-tolyl)porphyrinato) and [Mo(NHNPh$_2$)(NNPh$_2$)(acac)Cl$_2$] (acac: acetylacetonate).[12] For the latter two examples, M–$N_\alpha$ bond lengths of 1.911(3) and 1.948(5) Å and M-$N_\alpha$-$N_\beta$ angles of 141.1(3)° and 140.5(4)°, respectively, were found. This, along with the $N_\alpha$–$N_\beta$ bond lengths (Ru$N_\alpha$–$N_\beta$ 1.280(4) and Mo$N_\alpha$–$N_\beta$ 1.359(6) Å) indicates partial double-bond character for both the M–$N_\alpha$ and $N_\alpha$–$N_\beta$ bonds. In contrast, the Zr(1)–N(4) distance of 2.080(6) Å in **3a** is similar to those of the amido functions in the facially coordinating tripod ligand (Zr(1)–N(1) 2.037(6) Å, Zr(1)–N(2) 2.018(5) Å) and may therefore be viewed as a Zr–N single bond. Finally, the N(4)–N(5) bond length of 1.427(8) Å corresponds to a classical N–N single bond and is almost identical to the corresponding values found for the $\kappa^2$-hydrazido(1−) complexes [Zr($N_2^{TBS}N_{py}$)(NHNMe$_2$)Cl] and [Zr($N_2^{TBS}N_{py}$)(NHNMePh)Cl] (1.431(2) and 1.439(2) Å, respectively).[10]

The mixture of isomers of both **3a**,**b** and **4a**,**b** could be cleanly converted to the deep green diphenylhydrazido(2−) complexes [Zr($N_2^{TBS}N_{py}$)(NNPh$_2$)(py)] (**5**) and [Hf($N_2^{TBS}N_{py}$)(NNPh$_2$)(py)] (**6**), respectively, by dehydrohalogenation with lithium hexamethyldisilazide (LiHMDS) in the presence of one molar equivalent of pyridine. The formation of the linearly coordinated hydrazide in **5** and **6** is characterised by $^{15}$N NMR spectroscopy resonances of $\delta = 287.8$ ppm for Zr=$N_\alpha$ ($\delta = 289.1$ ppm for Hf=$N_\alpha$) and 178.2 ppm for the $N_\beta$Ph$_2$ nuclei in **5** (173.6 ppm in **6**). The molecular structure of **5** was established by X-ray diffraction[8] and is depicted in Figure 3.

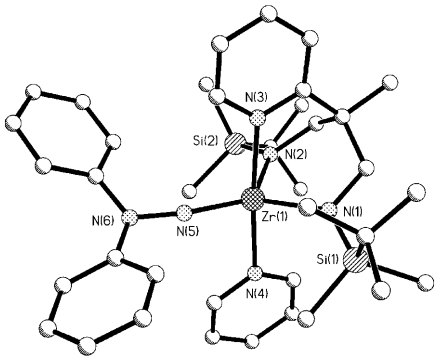


Figure 3. Molecular structure of complex **5**. Selected bond lengths [Å] and angles [°]: Zr(1)–N(1) 2.121(3), Zr(1)–N(2) 2.165(2), Zr(1)–N(3) 2.256(2), Zr(1)–N(4) 2.303(2), Zr(1)–N(5) 1.899(2), Si(1)–N(2) 1.755(3), N(5)–N(6) 1.398(3); N(1)-Zr(1)-N(2) 104.20(9), N(1)-Zr(1)-N(3) 81.73(9), N(1)-Zr(1)-N(4) 96.42(9), N(1)-Zr(1)-N(5) 126.00(11), N(2)-Zr(1)-N(3) 83.45(9), N(2)-Zr(1)-N(4) 91.30(9), N(2)-Zr(1)-N(5) 128.16(10), N(3)-Zr(1)-N(4) 173.79(9), N(3)-Zr(1)-N(5) 91.04(9), N(4)-Zr(1)-N(5) 94.82(10), Zr(1)-N(5)-N(6) 172.7(2).

Its overall molecular structure is best described as approximately trigonal bipyramidal with the pyridyl fragment of the tridentate ligand and the pyridine molecule occupying the axial positions (Zr(1)–N(3) 2.256(2), Zr(1)–N(4) 2.303(2) Å). The pyridyl N–Zr bond Zr(1)–N(3) is unusually short (2.256(2) Å) compared with that in **3a** and to other hydrazido(1−) zirconium complexes for which values between 2.441 and 2.451 Å were observed for this ligating unit.[10] As will be discussed below, the stretching mode associated with this bond is remarkably soft, and such a distortion may thus be associated with only a small energy incre-

  

ment. The two amido functions and the almost linearly coordinated diphenylhydrazido(2−) ligand are coordinated to the equatorial sites in **5**. The Zr(1)−N(5) bond length of 1.899(2) Å and the N(5)−N(6) distance of 1.398(3) Å as well as the Zr(1)-N(5)-N(6) angle of 172.7(2)° are similar to the corresponding metric parameters found in $[Cp_2Zr(N_2Ph_2)(dmap)]$ (1.873(7), 1.364(10) Å, 174.4(3)°, respectively)[5] and close to those found for the pyridiniumimido–zirconium complex $[Zr(N_2{}^{TBS}N_{py})(NNC_5H_5)(OTf)(py)]$ recently reported by us (1.945(3), 1.321(4) Å, 171.4(3)°, respectively).[13]

**The bonding capability of the hydrazido ligand**: To gain insight into the bonding of the hydrazinediido ligand in $[Zr(N_2{}^{TBS}N_{py})(NNPh_2)(py)]$ (**5**) a theoretical study of this complex using DFT and the B3PW91 functional has been carried out.[14] In general, good agreement of the computed local minimum **5x** with the experimentally determined structural data was obtained (Figure 4 and Table 1), however, a significant deviation (0.122 Å) is found for the Zr(1)−N(3) bond length of the ancillary tripod. It had been noted above, that the experimentally determined value in **5** is different from the corresponding values for related species. Evaluation of the dependence of the potential energy on the Zr(1)−N(3) bond length gave a very flat potential minimum for this stretching motion, with a difference of approximately 1 kcal mol$^{-1}$ in energy between the computed equilibrium geometry and the value determined experimentally.

A detailed investigation of the conformational space of complex **5** revealed a large number (18) of local minima (conformers) that differ in the orientation of the *tert*-butyldimethylsilyl groups, the hydrazido-$N_\beta$-bonded phenyl groups and the orientation of the hydrazinediido unit around the N−N=Zr axis. These conformers differ by $\Delta E \leq 0.9$ kcal mol$^{-1}$ ($\Delta G \leq 2.7$ kcal mol$^{-1}$); they are only separated by shallow barriers and are therefore assumed to be in equilibrium with each other.

As indicated above, the main aim of this part of the work is to rationalise the observed reactivity of **5** in relation to the bonding in the Zr–hydrazido unit and to evaluate its potential amphiphilic nature. Only a few previous computational studies analysing M–hydrazido fragments have been reported to date.[9] Notably, the titanium–diphenylhydrazido interaction in the complex $[Ti(NNPh_2)Cl_2\{HC(Me_2\text{-}pz)_3\}]$ (pz: pyrazolyl) has been studied in detail by Mountford et al.[1e] We chose to carry out a natural linear molecular orbital (NLMO) analysis[15] of **5x**. This approach was taken since the chemical interpretation of "Cartesian" (Kohn–Sham) molecular orbitals (CMO) is limited by the symmetry-imposed delocalisation. Whereas natural bond orbital (NBO) analyses provide localised orbitals, NLMO analyses give a semi-localised picture and interpretation of the bonding, offering direct insight into the nature of the "delocalisation tails".

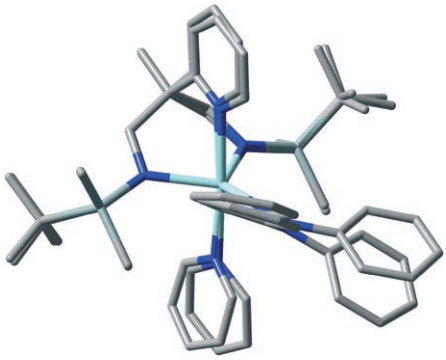

Figure 4. DFT-optimised molecular geometry of complex **5x** compared with the experimentally determined structure.

Table 1. Comparison of selected metric parameters experimentally determined for complex **5** and computed for the model compound **5x** (DFT-B3PW91).

| | Exptl (**5**) | Calcd (**5x**) |
|---|---|---|
| $d$(Zr(1)−N(5)) | 1.899 | 1.898 |
| $d$(N(5)−N(6)) | 1.398 | 1.366 |
| $d$(Zr(1)−N(2)) | 2.165 | 2.132 |
| $d$(Zr(1)−N(1)) | 2.121 | 2.114 |
| $d$(Zr(1)−N(3)) | 2.256 | 2.342 |
| $d$(Zr(1)−N(4)) | 2.302 | 2.424 |
| $\alpha$(Zr(1)-N(5)-N(6)) | 172.7 | 170.5 |
| $\alpha$(N(2)-Zr(1)-N(1)) | 104.2 | 103.2 |
| $\alpha$(N(3)-Zr(1)-N(4)) | 173.8 | 172.8 |

To facilitate the NLMO visualisation, a "stripped" version of the complex has been investigated in which the $N_2{}^{TBS}N_{Py}$ tripod is reduced to $HC(CH{=}NH)(CH_2NSiH_3)_2$, the phenyl substituents of the hydrazido group are replaced by H and the axial pyridine by $NHCH_2$. The results of this study, inserted for clarity into the frames of the full molecular structures, are depicted in Figure 5.

The σ bonding of the $N_2{}^{TBS}N_{py}$ ligand to the metal centre is mainly described by the NLMO orbitals 49A, 50A and 51A resulting in three highly polar bonding interactions with Zr (the designation A following the orbital number indicates the absence of symmetry restraints). In these orbital interactions the contribution of the metal to the Zr−N bond lies between 9 and 10%, thus reflecting the polarisation towards the electronegative ligating nitrogen atoms. The same applies to the fourth σ bond involving one of the spectator ligands in this complex (NLMO 52A), that is, the interaction of the axial pyridine ligand with the metal centre (7% contribution of Zr). In addition to the σ bonding, NLMOs 62A and 63A represent the highly polar π-bonding components of the bonding of the two amido donor functions (7% contribution of Zr).

Three frontier orbitals remain available for bonding ($1\times\sigma$, $2\times\pi$) to the hydrazinediido ligand (NLMOs 36A, 64A and 65A). The low-lying σ-bonding orbital of the $NNPh_2$ ligand (36A) represents a strong covalent interaction with the metal centre, with a 14% contribution from Zr. One π-bonding orbital (64A) represents a strong interaction between $N_\alpha$ and Zr, the contribution of the metal to the bond being 22%. The second, orthogonal π bond (65A) is again more strongly polarised towards the nitrogen (20% contri-

  

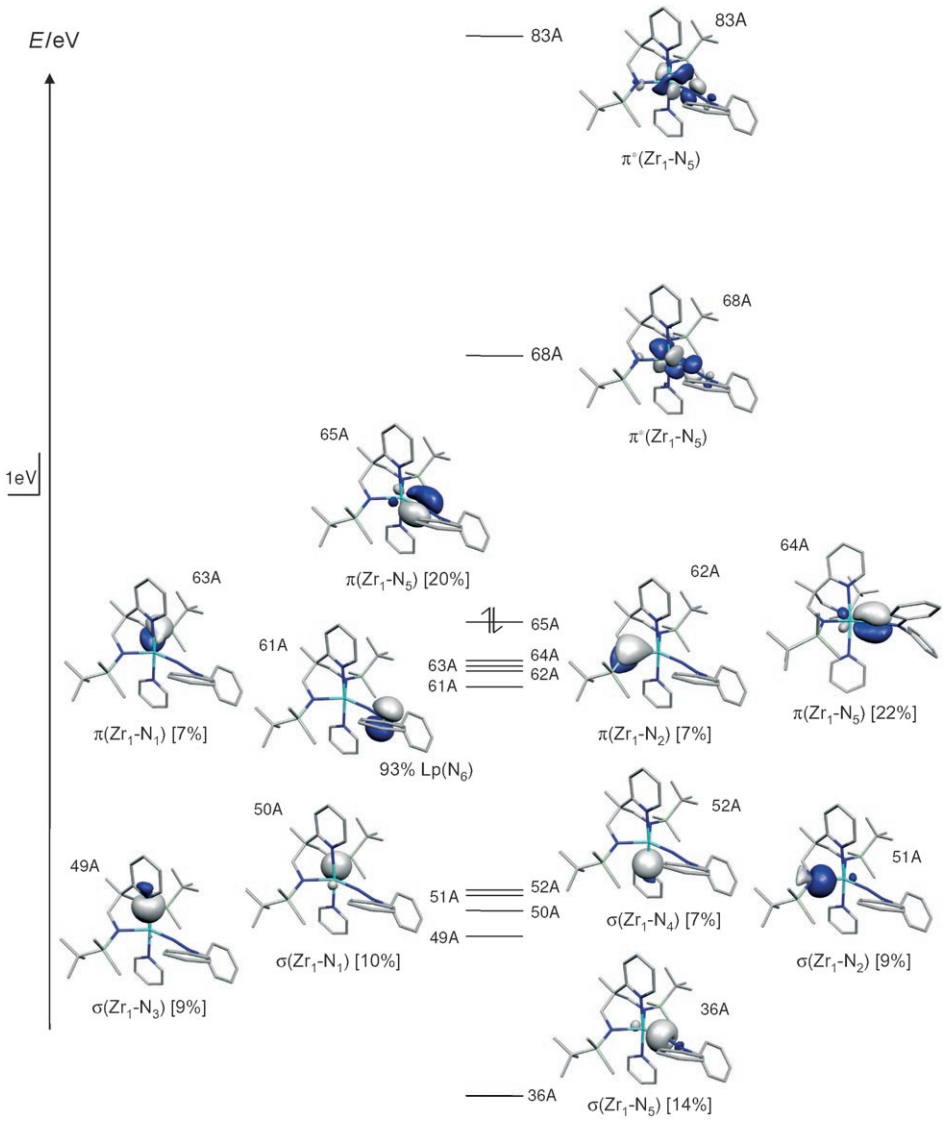


Figure 5. Selected frontier orbitals of a "stripped" version of complex **5x**. The calculated orbitals are inserted for clarity into the frames of the full molecular structures. The designation A following the orbital number indicates the absence of symmetry restraints.

bution of Zr). These results are in accordance with the bonding analysis for the $NNPh_2$ unit in $[Ti(NNPh_2)Cl_2\{HC(Me_2\text{-}pz)_3\}]$ reported previously.[11] Given the high polarity of the Zr=N bond, the hydrazinediide(2−) may be appropriately described as a six-electron donor ligand.

**Liberating a coordination site—decoordination of the axial pyridine ligand in $[Zr(N_2^{TBS}N_{py})(NNPh_2)(py)]$ (5)**: The pyridine ligand in $[M(N_2^{TBS}N_{py})(NNPh_2)(py)]$ (M = Zr: **5**, Hf: **6**) is substitutionally labile. This has been established in detail for complex **5** by a variable-temperature $^1H$ NMR spectroscopy study monitoring the exchange with one molar equivalent of free pyridine. Line-shape analysis of the dynamic spectra, recorded in $[D_8]$THF revealed a free activation enthalpy for the process of $\Delta G^{\neq} = 19$ kcal mol$^{-1}$. Given the patterns of reactivity established for the hydrazido as well as the corresponding imido complexes, the decoordination of the axially bonded pyridine ligand appears to play an important role as initial reactive step, a notion that has been previously backed up by detailed kinetic studies of reactions involving the corresponding imides.[16] It has also been possible to isolate and fully characterise such four-coordinate species in the case of the imidotitanium derivatives $[Ti(N_2^{TMS}N_{py})(NR)]$ (R = *t*Bu, mesityl) bearing the analogous trimethylsilyl-substituted tripodal diamido-pyridyl ligand.[7b]

In view of the importance of the liberation of the pyridine-substituted axial position in complex **5** as an initial step in its reactions with unsaturated substrates, we included this aspect in our computational study of **5x** and its derivatives. The geometrical optimisation of the corresponding four-coordinate complex structure of $\mathbf{5x}^{(-py)}$ without the axial pyridine ligand gave a local minimum structure that is 7.7 kcal mol$^{-1}$ higher in free energy with respect to **5x** ($\Delta E = 20.0$ kcal mol$^{-1}$, $\Delta H_{(298)} = 17.9$ kcal mol$^{-1}$, $T\Delta S_{(298)} = 10.2$ kcal mol$^{-1}$, $\Delta G_{(298)} = 7.7$ kcal mol$^{-1}$). We note the large modelled entropic term, which effectively reduces the free energy by 10.2 kcal mol$^{-1}$ with respect to the purely energetic contribution (at $P = 1$ atm and $T = 298.15$ K). However, addition of the solvent effects in the modelling (single-point calculation with polarised continuum method (PCM; THF)) increases $\Delta G_{(298)}$ again by 6 kcal mol$^{-1}$. Solvent effects thus play an important role, and the calculated energetic data should therefore be viewed as estimates.

The distorted trigonal-pyramidal geometry of the optimised $\mathbf{5x}^{(-py)}$ structure is characterised by a coordination vacancy in the axial position (Scheme 2). An investigation of the conformational space of $\mathbf{5x}^{(-py)}$ again revealed the possibility of several molecular conformers, the system represented in Scheme 2 being the one with the computed minimum free energy. The absence of pyridine in the complex leads to a decrease of the N–Zr bond lengths (Table 2), the effect being most pronounced for the *trans*-axial pyridyl-N of the

  

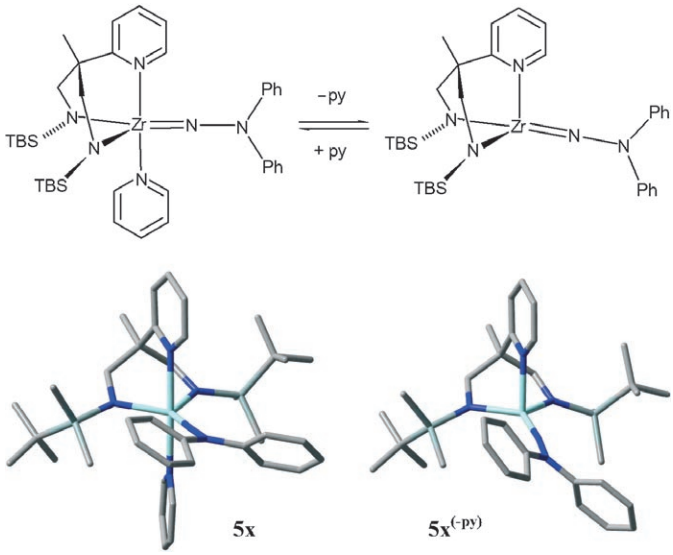


Scheme 2. Dissociation of the axial pyridine ligand in complex **5**. Computed molecular structures of the four-coordinate complex **5x** and the four-coordinate complex $\mathbf{5x}^{(-py)}$.

$N_2$Npy ligand ($\Delta d = -0.044$ Å). Overall, the minimum structure is characterised by a distortion from trigonal-pyramidal to tetrahedral coordination geometry, whereas the $NNPh_2$ fragment retains its linearity (Zr(1)-N(5)-N(6) = 173.3°). Analysis of the potential energy surface (PES) gave an estimate of the $\Delta E$ and $\Delta G$ values (c.a. 16 kcal mol$^{-1}$ and c.a. 15 kcal mol$^{-1}$ at 298 K, respectively) of the dissociation process, which are of similar magnitude and thus consistent with the free activation enthalpy of the pyridine exchange process derived from NMR spectroscopy line-shape analysis.

**Bonding and bending—the possibility of forming a side-on bound hydrazide**: A key point in the theoretical modelling of **5x** and its four-coordinate derivative $\mathbf{5x}^{(-py)}$ is the potential change in hapticity of the hydrazido unit from $\kappa^1$ to $\kappa^2$. In general, the bending of the hydrazido ligand can lead to two different arrangements that represent local energy minima: one in which the $NPh_2$ group is bent towards the pyridyl unit of the tripod ($\mathbf{5x}_{up}$ and $\mathbf{5x}^{(-py)}_{up}$), the other, in which it points in the opposite direction, $\mathbf{5x}_{down}$ and $\mathbf{5x}^{(-py)}_{down}$, respectively. The four computed minimum structures bearing the bent hydrazido units are depicted in Figure 6 and their characteristic metric parameters are listed in Table 3.

The principal difference between the linear and the bent hydrazido complexes is obviously reflected in the Zr(1)-N(5)-N(6) angles and Zr(1)−N(6) distances. For the former the transition from linear to bent is accompanied by a change from around 180 to 83–95°. For three of the four isomeric structures, $\mathbf{5x}_{up}$, $\mathbf{5x}_{down}$ and $\mathbf{5x}^{(-py)}_{up}$, the Zr(1)−N(6) distances are in the range of 2.300–2.376 Å, which is typical for tertiary amine coordination. On the other hand, the hydrazide in $\mathbf{5x}^{(-py)}_{down}$ adopts a somewhat different arrangement: a Zr(1)−N(6) distance of 2.493 Å, which indicates only a slight interaction of the $N_\beta$ atom with the metal and a dihedral angle N(3)-Zr(1)-N(5)-N(6) of −133.7°, which differs from the corresponding values of close to 0 or 180° in the other species. We assume that this particular arrange-

Table 2. Selected computed bond lengths [Å] and angles [°] for complex $\mathbf{5x}^{(-py)}$.

| | | | |
|---|---|---|---|
| $d$(Zr(1)−N(5)) | 1.888 | $d$(Zr(1)−N(1)) | 2.089 |
| $d$(N(5)−N(6)) | 1.361 | $d$(Zr(1)−N(3)) | 2.271 |
| $d$(Zr(1)−N(2)) | 2.088 | | |
| $\alpha$(Zr(1)-N(5)-N(6)) | 173.3 | $\alpha$(N(2)-Zr(1)-N(1)) | 105.8 |

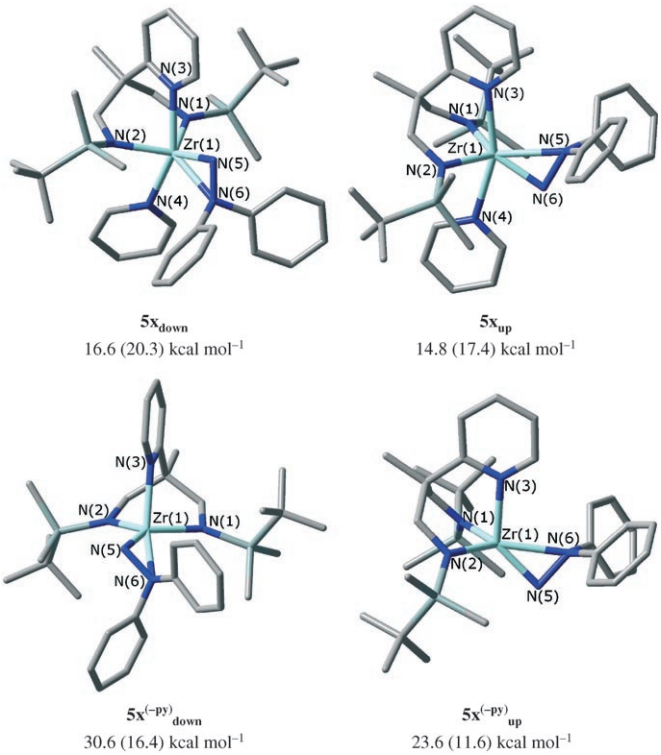


Figure 6. Full DFT-optimised structures derived from **5x** and $\mathbf{5x}^{(-py)}$ with $\kappa^2$ coordination of the hydrazido unit. Energies and free enthalpies (in kcal mol$^{-1}$) are given in parenthesis relative to **5x**.

Table 3. Selected computed bond lengths [Å] and angles [°] for the $\kappa^2$-hydrazido complexes.

| | $\mathbf{5x}_{down}$ | $\mathbf{5x}_{up}$ | $\mathbf{5x}^{(-py)}_{down}$ | $\mathbf{5x}^{(-py)}_{up}$ |
|---|---|---|---|---|
| $d$(Zr(1)−N(5)) | 1.960 | 1.963 | 1.911 | 1.929 |
| $d$(Zr(1)−N(6)) | 2.300 | 2.376 | 2.493 | 2.333 |
| $d$(Zr(1)−N(2)) | 2.142 | 2.114 | 2.078 | 2.095 |
| $d$(Zr(1)−N(1)) | 2.139 | 2.123 | 2.125 | 2.085 |
| $d$(Zr(1)−N(3)) | 2.363 | 2.393 | 2.285 | 2.315 |
| $d$(Zr(1)−N(4)) | 2.461 | 2.506 | – | – |
| $d$(N(5)−N(6)) | 1.436 | 1.434 | 1.433 | 1.437 |
| $\alpha$(Zr(1)-N(5)-N(6)) | 83.7 | 87.325 | 95.3 | 86.4 |
| $\alpha$(N(2)-Zr(1)-N(1)) | 110.0 | 102.805 | 103.7 | 99.0 |
| $\alpha$(N(3)-Zr(1)-N(4)) | 153.1 | 159.729 | – | – |
| $\theta$(N(3)-Zr(1)-N(5)-N(6)) | 178.3 | −16.3 | −133.7 | −18.2 |
| $\theta$(N(5)-Zr(1)-N(4)-$C_{Ar}$) | −60.4/126.4 | −9.7/171.9 | – | – |

ment is mainly due to inter-ligand repulsion within the complex. The transition states linking the $\kappa^1$ and $\kappa^2$ forms of **5x** and $\mathbf{5x}^{(-py)}$ have been determined and the activation barriers between the linear and bent forms were found to be below 6 kcal mol$^{-1}$ (Figure 7).

The relative free energies (in bold, along with the energies in brackets) of all six species, **5x** and $\mathbf{5x}^{(-py)}$ (middle), $\mathbf{5x}_{down}$ and $\mathbf{5x}^{(-py)}_{down}$ (left) as well as $\mathbf{5x}_{up}$ and $\mathbf{5x}^{(-py)}_{up}$ (right) are depicted in Figure 7. Also represented are the transition states connecting linear and bent species. The ground state of **5x** has been chosen as the origin in this representation. Regarding only the relative energies, those of $\mathbf{5x}^{(-py)}$ (19.9 kcal mol$^{-1}$) and the bent $\mathbf{5x}^{(-py)}_{up}$ (23.6 kcal mol$^{-1}$) are very close to each other and are only separated by a shallow activation barrier of approximately 10 kcal mol$^{-1}$ in the one direction and 6.5 kcal mol$^{-1}$ in the reverse direction. This appears to support a rapid interconversion of these species, a process that is thought to happen early on in the N–N scission in the presence of coupling reagents. It is also interesting to note that in terms of their relative energies the four-coordinate bent hydrazides appear to be disfavoured relative to their pyridine adduct, whereas in terms of the free energies this is reversed. The translational entropy of the ejected pyridine makes the bent four-coordinate species thermodynamically more favourable (see above).

**Representation of the key frontier orbitals on the side-on bound hydrazide plus partial charges**: An NLMO-based frontier orbital analysis of linear and bent isomers of the four-coordinate complex $\mathbf{5x}^{(-py)}$ can be used to elucidate the influence of the bending of the hydrazido unit on the electronic structures of $\mathbf{5x}^{(-py)}_{down}$ and $\mathbf{5x}^{(-py)}_{up}$. In Figure 8, the frontier orbitals representing the metal–hydrazide bonding and antibonding interactions are represented for the three species: In the centre, the Zr–N frontier orbitals of the linear hydrazide $\mathbf{5x}^{(-py)}$ are shown, whereas the left column represents the corresponding NLMOs of $\mathbf{5x}^{(-py)}_{down}$ and the right column those of the other bent isomer $\mathbf{5x}^{(-py)}_{up}$.

The main Zr–$N_\alpha$ bonding interactions in the linear complex $\mathbf{5x}^{-py}$ (central column of Figure 8) are represented by the polarised $\sigma$(Zr–$N_\alpha$) orbital 31A (14% contribution of Zr) and the two $\pi$(Zr–$N_\alpha$) bonding orbitals 56A and 57A (27 and 17% contributions of Zr, respectively), whereas the Zr–$N_\alpha$ antibonding combinations are the $\sigma$(Zr–$N_\alpha$) 78A and $\pi$(Zr–$N_\alpha$) 60A and 59A antibonding orbitals.

As to be expected, the $\sigma$(Zr–$N_\alpha$) 31A and the $\pi$(Zr–$N_\alpha$) 56A NLMO orbitals of the linear $\mathbf{5x}^{(-py)}$ are "mixed" in the bent compounds $\mathbf{5x}^{(-py)}_{down}$ and $\mathbf{5x}^{(-py)}_{up}$ (left and right column in Figure 8, respectively). In general the orbital lobes of the frontier orbitals are distorted in a way that facilitates a potential external attack at the $N_\alpha$ position. In the case of $\mathbf{5x}^{(-py)}_{down}$ (left column of Figure 8) the corresponding "mixed" orbitals are $\sigma$(Zr–$N_\alpha$) 44A (higher in energy that 31A) and the $\pi$(Zr–$N_\alpha$) orbital 52A (lower in energy that 56A). The same behaviour is found for complex $\mathbf{5x}^{(-py)}_{down}$ (right column of Figure 8), the corresponding orbitals being $\sigma$(Zr–$N_\alpha$) 42A (higher in energy that 31A) and $\pi$(Zr–$N_\alpha$) 54A (lower in energy that 56A). On the other hand, the $\pi$(Zr–$N_\alpha$) HOMO orbital (57A) in the linear and the two bent isomers is barely affected by the structural changes.

As for the two low-energy antibonding $\pi^*$(Zr–$N_\alpha$) orbitals 59A and 60A, the former is significantly destabilised in $\mathbf{5x}^{(-py)}_{down}$ (64A) and $\mathbf{5x}^{(-py)}_{up}$ (76A), whereas the latter is

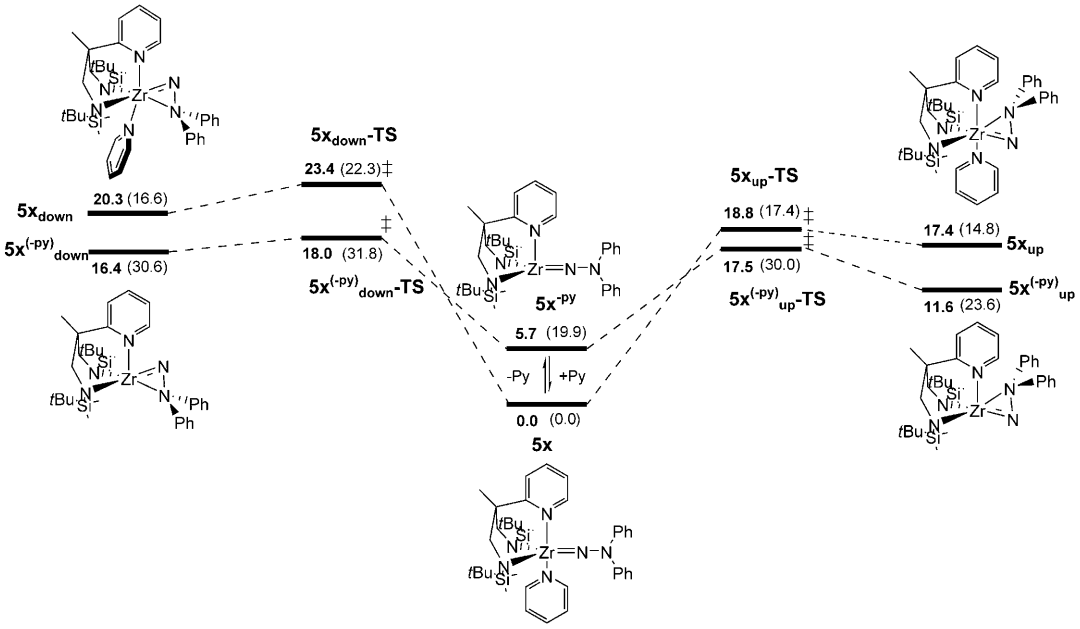


Figure 7. Pyridine decoordination and bending in compound **5x** (full DFT). All values correspond to the free energy referenced to the energy of **5x** ($\Delta E$ in parentheses). All energies are given in kcal mol$^{-1}$.

  

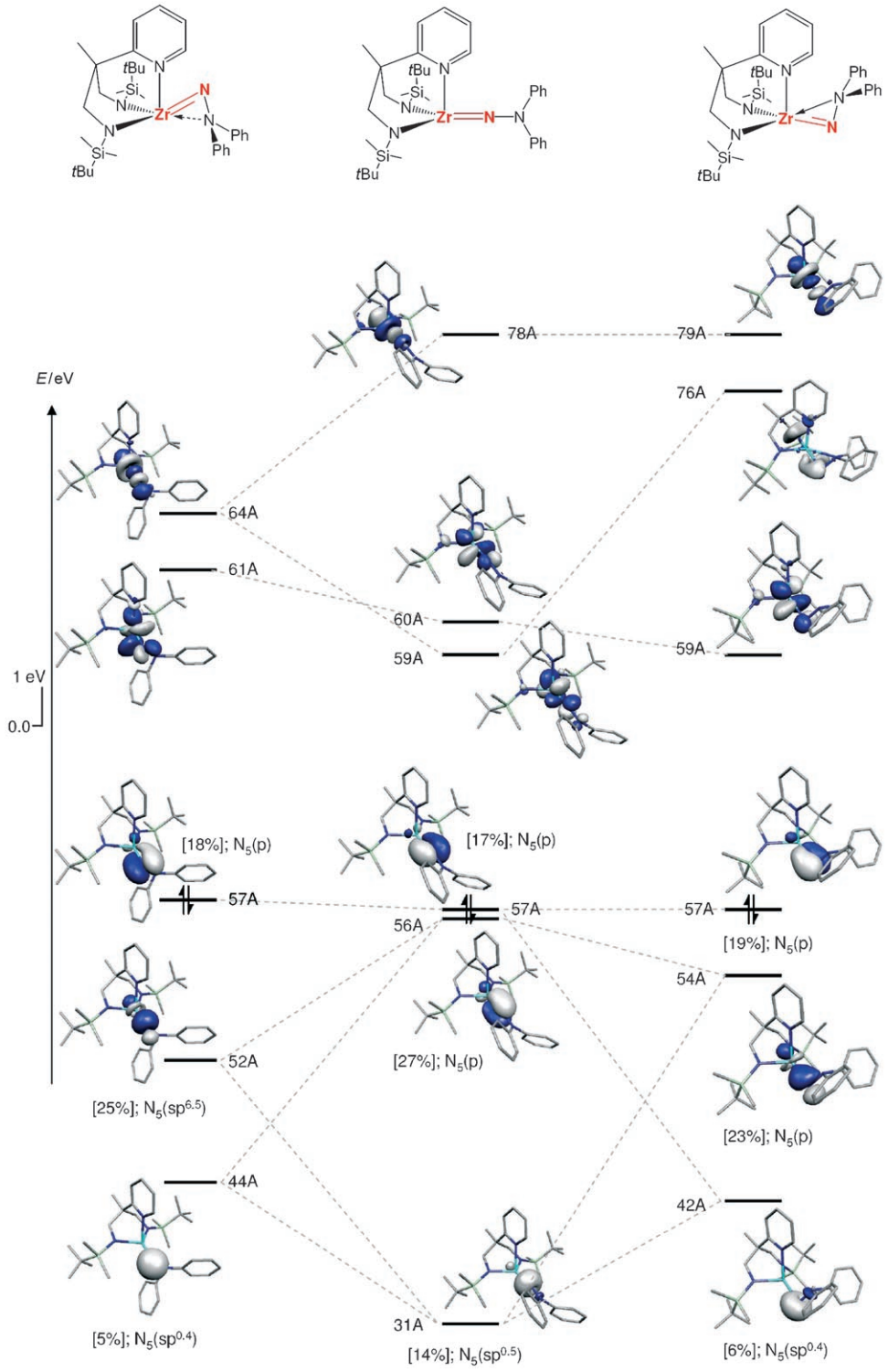


Figure 8. The frontier orbitals representing the metal–hydrazide bonding and antibonding interactions of the linear hydrazide $\mathbf{5x}^{(-py)}$ (centre) as well as the two bent species $\mathbf{5x}^{(-py)}_{down}$ (left) $\mathbf{5x}^{(-py)}_{up}$ (right). The contributions of the Zr atoms to the interactions are given in brackets. The designation A following the orbital number indicates the absence of symmetry restraints.

correlated with the energetically barely altered 61A and 59A in $\mathbf{5x}^{(-py)}_{down}$ and $\mathbf{5x}^{(-py)}_{up}$, respectively.

In Figure 9 the $\sigma(N_\alpha–N_\beta)$ and $\sigma^*(N_\alpha–N_\beta)$ frontier orbital interactions in the linear and bent hydrazido compounds $\mathbf{5x}^{(-py)}$, $\mathbf{5x}^{(-py)}_{down}$ and $\mathbf{5x}^{(-py)}_{up}$ are displayed. Notably, the $\sigma^*(N_\alpha–N_\beta)$ energy decreases in energy from the linear to the bent species, whereas the $\sigma(N_\alpha–N_\beta)$ bonding orbital is slightly destabilised.

Carrying out natural population analysis (NPA)[17] of the principal isomeric structures discussed above has provided the partial atomic charges within the complexes represented in Figure 10. Comparing the linear and bent hydrazido species, the charge at the Zr atom, in particular, becomes more positive for the latter ($\Delta q$ between $+0.09e$ and $+0.18e$), whereas the $N_\beta$ atom accumulates more negative charge upon bonding to zirconium ($\Delta q$ between $-0.16e$ and $-0.19e$). On the other hand, only minor modifications are found for the negatively charged $N_\alpha$ ($q$ from $-0.88e$ to $-0.96e$), which becomes slightly more negative upon going from the linear to bent arrangement ($\Delta q$ between $-0.01e$ and $-0.03e$). This suggests that a primarily charge-controlled nucleophilic attack at $N_\alpha$ is unlikely, whereas interaction with an electrophile could play an important role.

**Synthesis and characterisation of a Lewis acid adduct of the zirconium hydrazide—structural characterisation of a bent hydrazinediide**: The possibility of bent hydrazinediido units in transition-metal complexes has been previously proposed by Schrock et al.[18] They have been proposed as intermediates in an $N_2$ reduction cycle involving the tungsten hydrazide $[Cp^*MMe_3(N_2H_2)]$ ($Cp^*$: $C_5Me_5$) based on NMR spectroscopy evidence obtained in solution. In the latter case, the $N_\alpha$ atom was readily protonated, which is testimony to its basic nature.

  

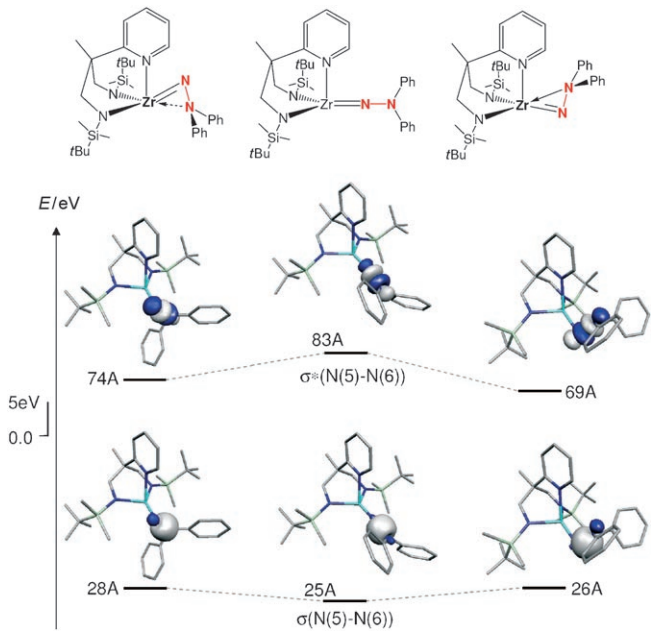


Figure 9. The $\sigma(N_\alpha–N_\beta)$ and $\sigma^*(N_\alpha–N_\beta)$ frontier orbital interactions in the linear and bent hydrazido compounds $\mathbf{5x}^{(-py)}$ (centre), $\mathbf{5x}^{(-py)}_{down}$ (left) and $\mathbf{5x}^{(-py)}_{up}$ (right).

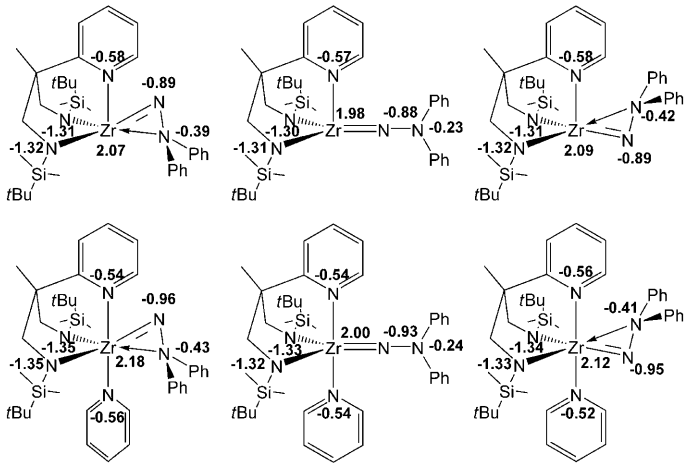

Figure 10. NPA partial charges of the six computed complexes $\mathbf{5x}$, $\mathbf{5x}^{(-py)}$, $\mathbf{5x}_{down}$, $\mathbf{5x}^{(-py)}_{down}$, $\mathbf{5x}_{up}$, and $\mathbf{5x}^{(-py)}_{up}$.

In view of Schrock's observations, complexes **5** and **6** were each reacted with one molar equivalent of $B(C_6F_5)_3$. Monitoring the reaction by using $^1$H NMR spectroscopy initially indicated the formation of the pyridine–$B(C_6F_5)_3$ Lewis acid–base adduct. Its $^{11}$B NMR spectroscopy signal was observed at $\delta=-3.4$ ppm, while the broad resonance at 60.6 ppm, assigned to free $B(C_6F_5)_3$, had disappeared. Within minutes, a second sharp resonance at −8.4 ppm grew in and a colourless crystalline solid began to precipitate. The $^1$H NMR spectra of the precipitates isolated after complete conversion of **5** and **6** displayed the characteristic resonance patterns of $C_s$ symmetric zirconium and hafnium complexes, **7** and **8**, similar to the reactants but without the resonances of the axial pyridine ligands. In both cases the $^{11}$B NMR spectra displayed the single sharp resonance at $\delta=-8.4$ ppm ($\Delta\nu_{1/2}=36$ Hz) already referred to above. The chemical shift range along with the small line width indicated the presence of a tetracoordinated boron compound of the $(Ar)_3B–NR_2$ type.[19] It was therefore presumed that the borane was coordinated to the hydrazido unit in [Zr-($N_2^{TBS}N_{py}$)(NNPh$_2$){$B(C_6F_5)_3$}] (**7**) and [Hf($N_2^{TBS}N_{py}$)-(NNPh$_2$){$B(C_6F_5)_3$}] (**8**) (Scheme 3).

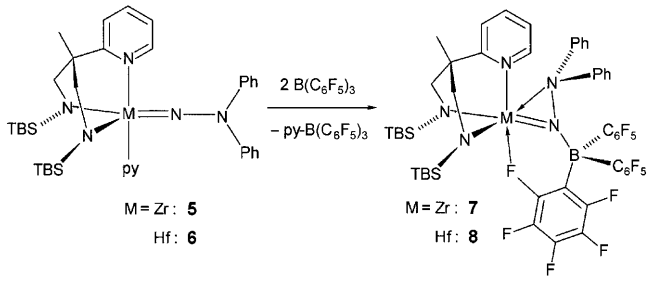


Scheme 3. Synthesis of the perfluorotriphenylborane adducts **7** and **8** of the hydrazinediido zirconium and hafnium complexes **5** and **6**, respectively. Electrophilic coordination to the $N_\alpha$ atom and formation of a bent hydrazinediide.

The $^{19}$F NMR spectra of both **7** and **8**, which were recorded at 293 K, displayed broad spectral features that represent an intermediate dynamic regime for the coordinated $B(C_6F_5)_3$ units. Lowering the temperature to 203 K rendered all fluorine nuclei non-equivalent. The $^{19}$F NMR spectrum of complex **8** recorded at that temperature is displayed in Figure 11 and shows the signals of 15 chemically non-equivalent nuclei in the chemical shift range between $\delta=-168.1$ and −119.8 ppm (the double intensity signal at −168.1 ppm being due to accidental spectral overlap).

Single crystals suitable for X-ray diffraction were obtained for both **7** and **8**. Two views of their molecular structures are depicted in Figure 12 along with the principal bond lengths and angles in the legend. Both compounds are not crystallographically isomorphous; however, their molecular structures are very similar. Therefore the discussion focuses on zirconium complex **7** (the corresponding data for the hafnium complex being given in brackets). The central metal atoms adopt pseudo-trigonal-bipyramidal coordination geometry, assuming that the side-on coordinated hydrazinediido ligand occupies one of the equatorial binding sites. The Zr(1)–N(4) (Hf–N(4)) bond length of 2.050(2) Å (2.039(2) Å) is close to the metal–N distances of the two amido functions of the ancillary tripod that occupy the other two equatorial positions, Zr(1)–N(1) 2.087(2) Å and Zr(1)–N(2) 2.058(2) Å (Hf–N(1) 2.067(2), Hf–N(2) 2.033(2) Å). On the other hand, the metal–N bond length of the $N_\beta$ atom of the hydrazinediide Zr(1)–N(5) 2.348(2) Å (Hf–N(5) 2.346(2) Å) is in the range of that of the pyridyl unit of the tripodal ligand: Zr(1)–N(3) 2.313(2) Å (Hf–N(3) 2.286(2) Å).

  

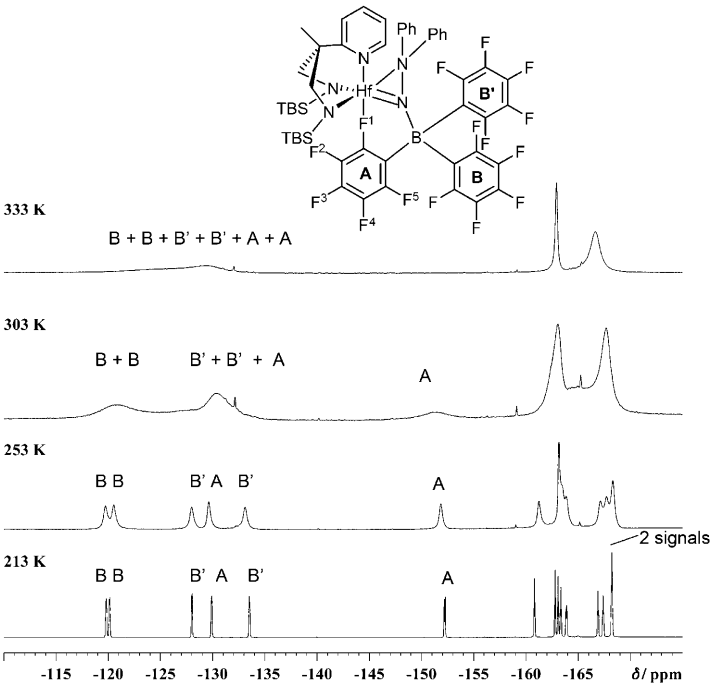


Figure 11. $^{19}$F NMR spectra of complex **8**. In the spectrum recorded at 213 K the signals of 15 magnetically non-equivalent nuclei in the chemical shift range between $\delta = -169.9$ and $-122.1$ ppm are displayed, the double intensity signal at $-168.1$ ppm is due to accidental spectral overlap.

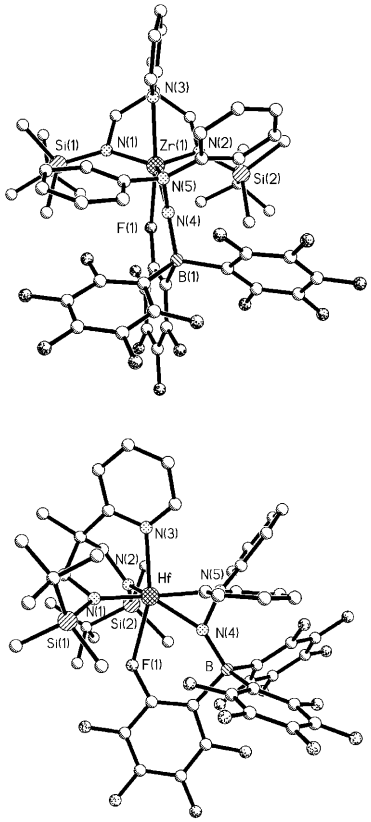


Figure 12. Top: Molecular structure of complex **7**. View within the plane defined by the side-on bound hydrazido unit. Selected bond lengths [Å] and angles [°]: Zr(1)–N(1) 2.087(2), Zr(1)–N(2) 2.058(2), Zr(1)–N(3) 2.313(2), Zr(1)–N(4) 2.050(2), Zr(1)–N(5) 2.348(2), N(4)–N(5) 1.459(3), Zr(1)–F(1) 2.393(1), N(4)–B(1) 1.573(3); N(1)-Zr(1)-N(2) 98.60(8), N(1)-Zr(1)-N(3) 82.83(7), N(1)-Zr(1)-N(4) 134.47(8), N(2)-Zr(1)-N(3) 88.60(7), N(2)-Zr(1)-N(4) 117.43(8), N(3)-Zr(1)-N(4) 122.37(7), N(4)-Zr(1)-N(5) 38.00(7), N(4)-N(5)-Zr(1) 59.88(10), N(5)-N(4)-Zr(1) 82.12(11), N(4)-Zr(1)-F(1) 72.27(6), N(5)-N(4)-B(1) 125.1(2). Bottom: Molecular structure of the corresponding hafnium complex **8**. View orthogonal to the hydrazide illustrating the intramolecular F–Hf coordination. Selected bond lengths [Å] and angles [°]: Hf–N(1) 2.067(2), Hf–N(2) 2.033(2), Hf–N(3) 2.286(2), Hf–N(4) 2.039(2), Hf–N(5) 2.346(2), Hf–F(1) 2.370(1), C(35)–F(1) 1.379(2), B–N(4) 1.562(3), N(4)–N(5) 1.468(2); N(1)-Hf-N(2) 99.36(7), N(1)-Hf-N(4) 133.36(7), N(1)-Hf-N(3) 82.36(7), N(3)-Hf-N(4) 123.87(6), N(1)-Hf-N(5) 135.08(6), N(3)-Hf-F(1) 161.68(5), Hf-N(4)-N(5) 82.3(1), Hf-N(5)-N(4) 59.42(9), Hf-F(1)-C(35) 138.1(1).

The $B(C_6F_5)_3$ group, which is attached to the $N_\alpha$ atom of the hydrazinediide in **7** and **8** adopts a conformation in which two perfluorophenyl rings point away from the metal centre whereas the third coordinates in an axial position (**7**: N(3)-Zr(1)-F(1) 165.10(6)°; **8**: N(3)-Hf-F(1) 161.68(5)°) through one of the *ortho*-fluorine atoms. The Zr(1)–F(1) and Hf–F(1) distances of 2.393(1) and 2.370(1) Å, respectively, lie between the extremes of metal–F covalent bonds (ca. 2 Å)[20] and pure van der Waals interactions (ca. 3.0 Å).[21] In the related betaine-type complex $[Cp_2Zr\{\eta^5\text{-}C_5H_4B(C_6F_5)_3\}]$ Erker and co-workers found a very similar Zr–F distance of 2.310(3) Å and a C-F-Zr angle of 138.0(3)°.[22] The corresponding values for **7** and **8** are 138.0(1) and 138.1(1)°, and are thus virtually identical. As a consequence of the coordination to the transition-metal centre, the C(35)–F(1) bond is slightly elongated (**7**: 1.385(3) Å; **8**: 1.379(2) Å) compared with the other 14 C–F bonds of the perfluorophenyl rings (average values 1.346 and 1.341 Å for **7** and **8**, respectively).

Given the bonding analysis for a "free" side-on bound hydrazide at zirconium presented in the previous section, it was of interest to find out to what degree the attachment of the Lewis acid influenced its structure and bonding. To this end a computational study of complex **7** was carried out. Its full DFT (B3PW91)-optimised geometry **7x** was found to be in good agreement with the experimental data obtained by X-ray diffraction (Figure 13 and Table 4), the only exception being again the Zr(1)–N(3) bond length of the axially bound pyridyl unit ($\Delta d = 0.063$ Å).

The principal NLMOs representing the bonding between the zirconium atom and the borane–hydrazido moiety are displayed in Figure 14. As is readily apparent, the double-bonding interaction with the hydrazido–$N_\alpha$ atom Zr(1)=N(4) ($\sigma$ and $\pi$) is represented in the two top frontier orbitals. Given the strong polarity of the Zr–N bonds, the Wiberg index associated with this interaction of 0.61 (Table 5) is as expected.[23] Highly polar, but significant donor–acceptor bonding interactions are also found for Zr(1)–N(5) and Zr(1)–F(1) (represented by the two NLMO frontier orbitals at the bottom of Figure 14), which are cor-

  

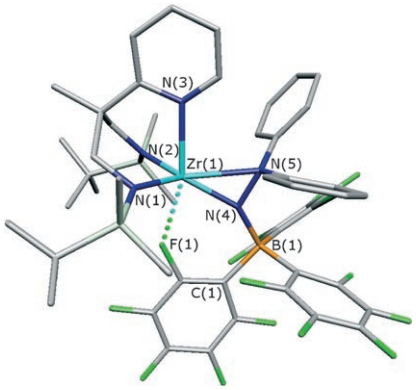


Figure 13. DFT-optimised molecular geometry of complex **7x**.

Table 4. Selected experimental and computed bond lengths [Å] and angles [°] for compound **7** and for the model compound **7x** (DFT-B3PW91).

| | Exptl (**7**) | Calcd (**7x**) |
|---|---|---|
| *d*(Zr(1)–N(4)) | 2.050 | 2.053 |
| *d*(Zr(1)–N(5)) | 2.348 | 2.385 |
| *d*(Zr(1)–N(1)) | 2.087 | 2.101 |
| *d*(Zr(1)–N(2)) | 2.058 | 2.063 |
| *d*(Zr(1)–N(3)) | 2.313 | 2.376 |
| *d*(Zr(1)–B(1)) | 1.573 | 1.587 |
| *d*(N(4)–N(5)) | 1.459 | 1.439 |
| *d*(Zr(1)–F(1)) | 2.392 | 2.358 |
| *α*(Zr(1)-N(4)-N(5)) | 82.2 | 84.2 |
| *α*(N(1)-Zr(1)-N(2)) | 98.6 | 100.1 |
| *α*(Zr(1)-N(3)-B(1)) | 152.7 | 150.1 |
| *α*(N(5)-N(4)-B(1)) | 125.0 | 125.4 |

roborated by the Wiberg indexes of 0.17 and 0.15 for these bonds, respectively (Table 5).[23] The key frontier orbitals representing the N–N bonding within the bent hydrazido unit are depicted in Figure 15. Closer inspection of the frontier orbital energies has revealed that the coordination of the $B(C_5F_6)_3$ at $N_\alpha$ has led to a slight stabilisation of the σ*(N–N) antibonding orbital relative to the complexes **5x** and $\mathbf{5x}^{(-py)}$ (by 0.1 eV).

A natural population analysis (NPA) of compound **7x** has been carried out to asses the influence that the Lewis acid coordination has upon the hydrazido ligand. Its comparison with $\mathbf{5x}^{(-py)}_{up}$ (Figure 16) reveals a significant modification of the partial charges on N(4) and N(5) upon coordination of $B(C_6F_5)_3$ to N(4). Furthermore, the partial positive charge on the Zr atom is increased (+2.33*e*) potentially rendering it more Lewis acidic.

**Thermal rearrangement of $[Zr(N_2^{TBS}N_{py})(NNPh_2)\{B(C_6F_5)_3\}]$ (7)—pentafluorophenyl migration to the metal centre**: Upon heating a solution of complex **7** at 65 °C a rearrangement to a new compound **9** was observed, which possesses an NMR spectroscopy signal pattern that is consistent with $C_s$ molecular symmetry. Based on the spectroscopic data, the structural assignment represented in Scheme 4 was derived.

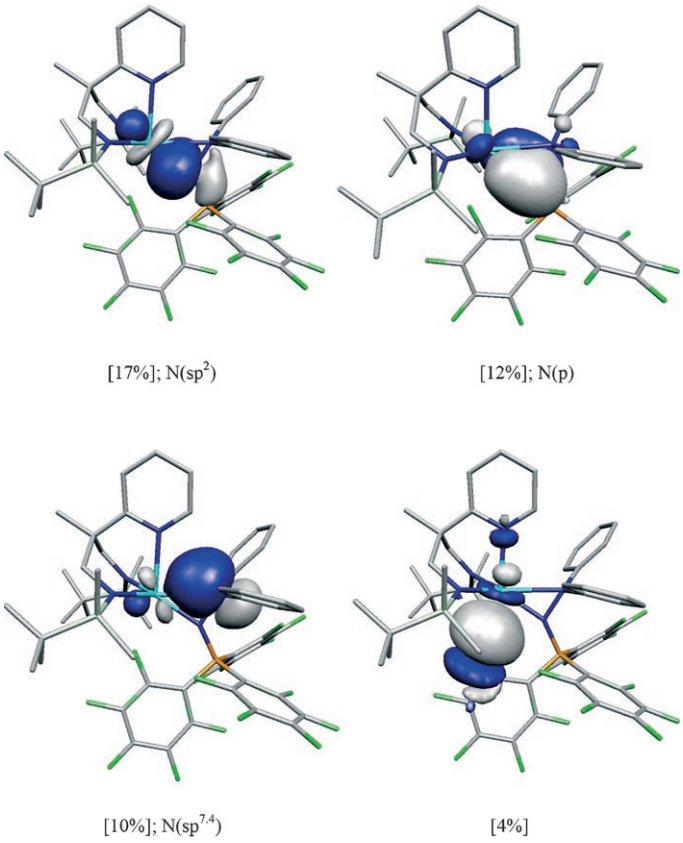


Figure 14. Representation of selected NLMO orbitals of compound **7x**. Values in brackets represent the contribution of the Zr atoms to the corresponding interaction.

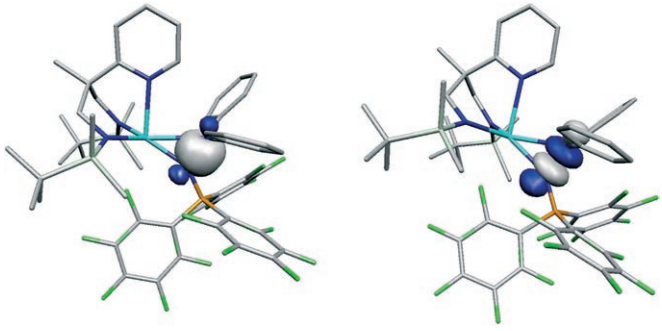

Figure 15. The N–N σ and σ* NLMO orbitals of compound **7x**.

Table 5. Selected Wiberg indices for complex **7**.

| | | | |
|---|---|---|---|
| Zr(1)–N(4) | 0.61 | N(4)–B(1) | 0.76 |
| Zr(1)–N(5) | 0.17 | Zr(1)–F(1) | 0.15 |
| N(4)–N(5) | 1.00 | B(1)–C(1) | 0.80 |

In the conversion of **7** to **9**, the sharp $^{11}B$ NMR signal at $\delta = -8.4$ ppm ($\Delta\nu_{1/2} = 36$ Hz) disappeared while a broad resonance at 36 ppm ($\Delta\nu_{1/2} = 545$ Hz) is growing in. The chemical shift range, along with the large line width are consistent with threefold coordination at the boron atom of the type

  

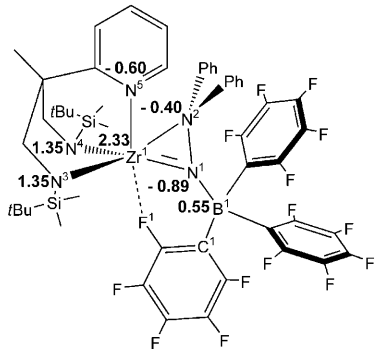


Figure 16. Natural population analysis of complex **7x**.

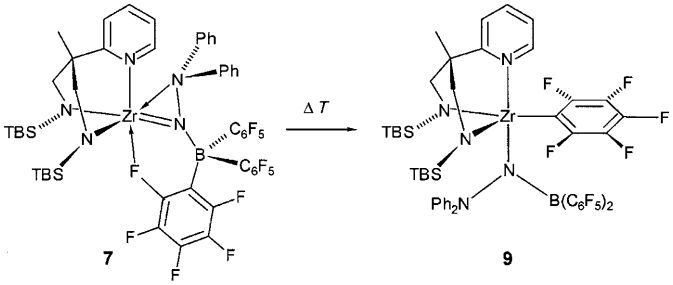


Scheme 4. Thermal rearrangement of the perfluorotriphenylborane adduct **7** by pentafluorophenyl migration to the Zr atom to give complex **9**.

$(Ar)_2B–NR_2$.[19] An N–N bond cleavage and migration of a diphenylamido unit to the metal can be ruled out on the basis of the $^1H$ and $^{15}N$ NMR spectroscopic data of **9**. The chemical shifts of the $N_\beta$ nuclei of the hydrazido unit in **9** at 119.3 ppm deviates significantly from such zirconium-bonded amido fragments, as observed from the N–N cleavage reaction (average $^{15}N$ NMR chemical shift of 191 ppm), whilst being close to the $^{15}N_\beta$ resonance in $[Zr(N_2{}^{TBS}N_{py})(NHNPh_2)Cl]$ (**3a+b**) ($\delta = 116.9$ and 104.5 ppm, respectively) reported in this work. The other NMR spectroscopic features of **9** support the structural assignment given in Scheme 4. The axial position of the boryl hydrazido group has been confirmed by NOE experiments showing close contacts of the *ortho*-H and *meta*-H atoms of the $NPh_2$ substituents with the *t*Bu groups. We note that there are several examples of degradative perfluorophenyl migrations from boranes to group 4 metal centres in the literature.[24] They represent a possible deactivation pathway in the catalytic polymerisation of alkenes. Similar behaviour has been observed for the hafnium analogue **8**, however, the thermal rearrangement proved to be less selective than that for **7**.

## Conclusion

This work has provided a comprehensive study of the synthesis, structures and bonding of a zirconium and, for the first time, a hafnium hydrazinediido complex. The previously proposed structural rearrangement of a linear end-on bound hydrazide(2–) to its bent $\kappa^2$-bonded isomer has been established as a thermally feasible transformation. The resulting more reactive N–N fragment has a frontier orbital structure that makes it more amenable to attacks by reagents of an amphiphilic nature. Experimental support for these findings obtained with theoretical methods comes from the preparation and structural characterisation of bent hydrazinediides of zirconium and hafnium stabilised by the Lewis acid $B(C_6F_5)_3$, which coordinates to the $N_\alpha$ atom. The extent that bent hydrazinediides play a role in the N–N bond cleavage and N–E coupling steps recently observed in several transformations is currently being investigated in our laboratory.

## Experimental Section

All manipulations of air- and moisture-sensitive materials were performed under an inert atmosphere of dry argon using standard Schlenk techniques or by working in a glove box. Solvents were dried over sodium (toluene), potassium (hexanes) or sodium/potassium alloy (pentane, diethyl ether); distilled and degassed prior to use. Deuterated solvents were dried over potassium ($C_6D_6$, [$D_8$]THF, [$D_8$]toluene), vacuum distilled and stored in Teflon valve ampoules under argon. Samples for NMR spectroscopy were prepared under argon in 5 mm tubes equipped with Teflon valves. NMR spectra were recorded on Bruker DRX 200, AvanceII 400 and AvanceIII 600 NMR spectrometers and were referenced internally by using the residual protio solvent ($^1H$) or solvent ($^{13}C$) resonances or externally to $BF_3OEt_2$ ($^{11}B$), $SiMe_4$ ($^1H$, $^{13}C$, $^{29}Si$), $CFCl_3$ ($^{19}F$) and $NH_{3(l)}$ ($^{15}N$). $^{15}N$ data were obtained by two-dimensional $^1H$ correlation experiments or by direct detection using a cryogenically cooled direct-detection NMR probe (QNP CryoProbe™). Elemental analyses were recorded by the analytical service of the Heidelberg Chemistry Department. The protioligand $H_2N_2N_{py}$ and the dichloro complex $[Zr(N_2{}^{TBS}N_{py})Cl_2]$ (**1**) were prepared according to published procedures.[7,8,10] All other reagents were obtained from commercial sources and used as received unless explicitly stated.

**Preparation of the complexes**

*Preparation of $[Hf(N_2{}^{TBS}N_{py})Cl_2]$ (**2**)*: 2.5 M *n*BuLi (5 mL, 12.5 mmol) was added slowly by syringe to a cooled (−78 °C) solution of $H_2N^{TBS}N_{py}$ (2.46 g, 6.2 mmol) in toluene (20 mL). The reaction mixture was stirred for 18 h at room temperature, and was transferred to a cooled (−78 °C) slurry of $HfCl_4$ in toluene. The reaction mixture was allowed to warm up and was stirred for an additional 18 h at room temperature. After filtration the volatiles were removed under reduced pressure, the residue was washed with diethyl ether (3×10 mL) and dried under vacuum to yield a colourless powder (1.25 g, 2.0 mmol, 33 %). Single crystals for X-ray diffraction were grown from a saturated solution in toluene at 10 °C. $^1H$ NMR (600 MHz, $C_6D_6$, 296 K): $\delta = 0.01$, 0.51 (s, 2×6H; $Si(CH_3)_2$), 0.83 (s, 18H; $SiC(CH_3)_3$), 0.88 (s, 3H; $CH_3$), 3.46 (d, $^2J_{HH} = 12.5$ Hz, 2H; CHH), 4.07 (d, $^2J_{HH} = 12.5$ Hz, 2H; CHH), 6.50 (ddd, $^3J_{H5pyH4py} = 7.7$ Hz, $^3J_{H5pyH6py} = 5.6$ Hz, $^4J_{H5pyH3py} = 1.2$ Hz, 1H; $H5_{py}$), 6.77 (d, $^3J_{H3pyH4py} = 8.0$ Hz, 1H; $H3_{py}$), 7.00 (dt, $^3J_{H4pyH5pyH3py} = 7.8$ Hz, $^4J_{H4pyH6py}$, 1H; $H4_{py}$), 9.56 ppm (dd, $^3J_{H6pyH5py} = 5.6$ Hz, $^4J_{H6pyH4py} = 1.1$ Hz, 1H; $H6_{py}$); $^{13}C\{^1H\}$ NMR (100 MHz, $C_6D_6$, 296 K): $\delta = -4.8$, −3.9 ($Si(CH_3)_2$), 20.9 ($Si–C(CH_3)_3$), 23.5 ($CH_3$), 27.5 ($Si–C(CH_3)_3$), 48.4 ($C–CH_3$), 62.4 ($CH_2$), 121.1 ($C3_{py}$), 122.5 ($C5_{py}$), 139.6 ($C4_{py}$), 148.0 ($C6_{py}$), 160.6 ppm ($C2_{py}$); $^{29}Si\{^1H\}$ NMR (80 MHz, $C_6D_6$, 296 K): $\delta = 3.38$ ppm ($Si(CH_3)_2tBu$); $^{15}N$ NMR (60 MHz, $C_6D_6$, 296 K): $\delta = 198.3$ ($N–Si(CH_3)_2tBu$), 283.5 ppm ($L–N_{py}$); IR (Nujol, NaCl): $\tilde{\nu} = 1606$ (s), 1569 (w), 1465 (s), 1377 (s), 1297 (w), 1248 (s), 1171 (m), 1145 (m), 1048 (s), 960 (w), 917 (sh), 863 (sh), 771 (sh), 672 (s), 606 $cm^{-1}$ (m); elemental analysis calcd (%) for $C_{20}H_{38}N_3Si_2Cl_2Hf$: C 39.34, H 6.45, N 6.55; found: C 39.79, H 6.41, N 6.56.

  

*Preparation of [Zr($N_2^{TBS}N_{py}$)(NHNPh$_2$)Cl] (**3a**) and (**3b**)*: A suspension of LiNHNPh$_2$ (1.17 g, 6.2 mmol, 1.2 equiv) in toluene (10 mL) was added dropwise over approximately 10 min to a stirred solution of [Zr($N_2^{TBS}N_{py}$)Cl$_2$] (2.82 g, 5.1 mmol) in toluene (50 mL). During the addition the clear colourless solution became cloudy and orange. The reaction was stirred for two days. The precipitated LiCl was removed by filtration and the volatiles were removed under reduced pressure. The crude product was extracted with pentane and filtered away from insoluble impurities. The solvent was removed from the extract under reduced pressure and the orange solid was finally washed with cold pentane. Yield: 2.50 g (3.6 mmol, 71 %). Single crystals for X-ray diffraction were grown from a saturated solution in toluene at 10 °C. $^1$H NMR (400 MHz, C$_6$D$_6$, 296 K) for **3a**: $\delta$ = −0.03, 0.12 (s, 2×6H; Si(C$H_3$)$_2$), 0.63 (s, 18H; Si−C(C$H_3$)$_3$), 0.98 (s, 3H; C$H_3$), 3.30 (d, $^2J_{HH}$ = 12.9 Hz, 2H; CH*H*), 3.88 (d, $^2J_{HH}$ = 12.8 Hz, 2H; C*H*H), 6.54 (s, 1H; N*H*), 6.55 (ddd, $^3J_{H5pyH4py}$ = 7.5 Hz, $^3J_{H5pyH6py}$ = 5.4 Hz, $^4J_{H5pyH3py}$ = 1.1 Hz, 1H; *H*5$_{py}$), 6.81 (d, $^3J_{H3pyH4py}$ = 8.0 Hz, 1H; *H*3$_{py}$), 6.89 (t, $^3J_{HpHm}$ = 7.3 Hz, 2H; *p*-*H*$_{Ph}$), 7.01 (dt, $^3J_{H4pyH3py/5py}$ = 7.8 Hz, $^4J_{H4pyH6py}$ = 1.8 Hz, 1H; *H*4$_{py}$), 7.26 (dd, $^3J_{HmHo}$ = 8.6 Hz, $^3J_{HmHp}$ = 7.3 Hz, 4H; *m*-*H*$_{Ph}$), 7.67 (dd, $^3J_{HoHm}$ = 8.7 Hz, $^4J_{HoHp}$ = 1.0 Hz, 4H; *o*-*H*$_{Ph}$), 9.56 ppm (ddd, $^3J_{H6pyH5py}$ = 5.4 Hz, $^4J_{H6pyH4py}$ = 1.7 Hz, $^5J_{H6pyH3py}$ = 0.6 Hz, 1H; *H*6$_{py}$); $^{13}$C{$^1$H} NMR (100 MHz, C$_6$D$_6$, 296 K) for **3a**: $\delta$ = −4.8, −4.7 (Si(C$H_3$)$_2$), 20.5 (*C*−CH$_3$), 24.1 (Si−C(C$H_3$)$_3$), 27.4 (Si−C(C$H_3$)$_3$), 48.7 (*C*−CH$_2$), 63.6 (C$H_2$), 119.8–123.0 (*o*-*C*$_{Ph}$, *p*-*C*$_{Ph}$, *C*3$_{py}$, *C*5$_{py}$), 128.9 (*m*-*C*$_{Ph}$), 138.6 (*C*4$_{py}$), 148.3 (*C*6$_{py}$), 151.6 (N−*C*$_{Ph}$), 160.9 ppm (*C*2$_{py}$); $^{29}$Si{$^1$H} NMR (80 MHz, C$_6$D$_6$, 296 K) for **3a**: $\delta$ = 1.5 ppm (*Si*(CH$_3$)$_2$*t*Bu); $^{15}$N NMR (60 MHz, C$_6$D$_6$, 296 K) for **3a**: $\delta$ = 116.9 (*N*Ph$_2$), 196.7 (*N*−Si(CH$_3$)$_2$*t*Bu), 203.6 ($^1J_{NH}$ = 63 Hz; *N*H), 290.7 ppm (*N*$_{py}$); $^1$H NMR (400 MHz, C$_6$D$_6$, 296 K) for **3b**: $\delta$ = 0.03, 0.46 (s, 6H; Si(C$H_3$)$_2$), 0.90 (s, 18H; Si−C(C$H_3$)$_3$), 1.0 (s, 3H; C$H_3$), 3.30 (d, $^2J_{HH}$ = 12.9 Hz, 2H; CH*H*), 4.05 (d, $^2J_{HH}$ = 12.8 Hz, 2H; C*H*H), 6.26 (ddd, $^3J_{H5pyH4py}$ = 7.4 Hz, $^3J_{H5pyH6py}$ = 5.4 Hz, $^4J_{H5pyH3py}$ = 1.1 Hz, 1H; *H*5$_{py}$), 6.31 (s, 1H; N*H*), 6.75 (d, $^3J_{H3pyH4py}$ = 8.0 Hz, 1H; *H*3$_{py}$), 6.91 (m, 2H; *p*-*H*$_{Ph}$), 6.93 (m, 1H; *H*4$_{py}$), 7.16 (m, 4H; *m*-*H*$_{Ph}$), 7.41 (dd, $^3J_{HoHm}$ = 8.6 Hz, $^4J_{HoHp}$ = 1.0 Hz, 4H; *o*-*H*$_{Ph}$), 8.09 ppm (dd, $^3J_{H6pyH5py}$ = 5.4 Hz, $^4J_{H6pyH4py}$ = 1.0 Hz, 1H; *H*6$_{py}$); $^{13}$C{$^1$H} NMR (100 MHz, C$_6$D$_6$, 296 K) for **3b**: $\delta$ = −4.5, −4.2 (Si−(C$H_3$)$_2$), 20.6 (Si−*C*(CH$_3$)$_3$), 24.1 (C−*C*H$_3$), 27.9 (Si−C(C$H_3$)$_3$), 48.7 (*C*−CH$_3$), 63.2 (C$H_2$), 119.8–123.0 (*o*-*C*$_{Ph}$, *p*-C$_{Ph}$, *C3*$_{py}$, *C5*$_{py}$), 129.1 (*m*-*C*$_{Ph}$), 138.6 (*C4*$_{py}$), 148.0 (*C6*$_{py}$), 153.1 (N−*C*$_{Ph}$), 161.4 ppm (*C2*$_{py}$); $^{29}$Si{$^1$H} NMR (80 MHz, C$_6$D$_6$, 296 K) for **3b**: $\delta$ = 2.0 ppm (*Si*(CH$_3$)$_2$*t*Bu); $^{15}$N NMR (60 MHz, C$_6$D$_6$, 296 K) for **3b**: $\delta$ = 104.5 (*N*Ph$_2$), 191.8 (*N*−Si(CH$_3$)$_2$*t*Bu), 211.7 ($^1J_{NH}$ = 63 Hz, *N*H), 287.4 ppm (*N*$_{py}$); IR (Nujol, NaCl) (mixture of the two isomers): $\tilde{\nu}$ = 3218 (w), 3062 (w), 2954 (m), 2922 (m), 2846 (m), 1597 (m), 1582 (s), 1484 (s), 1253 (m), 1057 (m), 854 (s), 768 (m), 729 (m), 702 (w), 668 (w), 633 (w), 597 cm$^{-1}$ (w); elemental analysis for the mixture of the two isomers calcd (%) for C$_{33}$H$_{52}$ClN$_5$Si$_2$Zr: C 56.49, H 7.47, N 9.98; found: C 56.43, H 7.43, N 10.05.

*Preparation of [Hf($N_2^{TBS}N_{py}$)(NHNPh$_2$)Cl] (**4a** and **4b**)*: A suspension of LiNHNPh$_2$ (0.30 g, 1.6 mmol) in toluene was added slowly to a stirred solution of [Hf($N_2^{TBS}N_{py}$)Cl$_2$] (1.00 g, 1.6 mmol) in toluene (10 mL). During the addition the clear colourless solution became cloudy and turned green. The reaction mixture was stirred for two days at room temperature. The precipitated LiCl was removed by filtration, and the crude product was extracted with pentane and filtered away from insoluble impurities. The solution was concentrated and the product crystallised at −20 °C to give pale yellow micro-crystals (1.01 g, 1.3 mmol, 81 %). $^1$H NMR (600 MHz, C$_6$D$_6$, 296 K) for **4a**: $\delta$ = −0.04, 0.15 (s, 6H; Si(C$H_3$)$_2$), 0.65 (s, 18H; Si−C(C$H_3$)$_3$), 0.93 (s, 3H; C$H_3$), 3.51 (d, $^2J_{HH}$ = 12.4 Hz, 2H; CH*H*), 3.93 (d, $^2J_{HH}$ = 12.4 Hz, 2H; C*H*H), 6.32 (s, 1H; N*H*), 6.52 (m, 1H; *H*5$_{py}$), 6.79 (d, $^3J_{H3pyH4py}$ = 8.0 Hz, 1H; *H*3$_{py}$), 6.91 (t, $^3J_{HpHm}$ = 7.1 Hz, 2H; *p*-*H*$_{Ph}$), 6.98 (dt, $^3J_{H4pyH3py/5py}$ = 7.7 Hz, $^4J_{H4pyH6py}$ = 1.6 Hz, 1H; *H*4$_{py}$), 7.28 (t, $^3J_{HmHoHp}$ = 7.8 Hz, 4H; *m*-*H*$_{Ph}$), 7.68 (d, $^3J_{HoHm}$ = 8.3 Hz, 4H; *o*-*H*$_{Ph}$), 9.51 ppm (dd, $^3J_{H6pyH5py}$ = 5.4 Hz, $^4J_{H6pyH4py}$ = 1.0 Hz, 1H; *H*6$_{py}$); $^{13}$C{$^1$H} NMR (100 MHz, C$_6$D$_6$, 296 K) for **4a**: $\delta$ = −4.7 (Si(C$H_3$)$_2$), 20.7 (Si−*C*(CH$_3$)$_3$), 23.9 (C−*C*H$_3$), 27.4 (Si−C(C$H_3$)$_3$), 48.0 (*C*−CH$_3$), 63.0 (C$H_2$), 120.8 (*o*-*C*$_{Ph}$), 122.1 (*C3*$_{py}$), 122.1–123.0 (*m*-*C*$_{Ph}$, *p*-*C*$_{Ph}$, *C5*$_{py}$), 138.8 (*C4*$_{py}$), 147.9 (*C6*$_{py}$), 151.9 (N−*C*$_{Ph}$), 161.2 ppm (*C2*$_{py}$); $^{29}$Si{$^1$H} NMR (80 MHz, C$_6$D$_6$, 296 K) for **4a**: $\delta$ = 2.23 ppm (*Si*(CH$_3$)$_2$*t*Bu); $^{15}$N NMR (60 MHz, C$_6$D$_6$, 296 K) for **4a**: $\delta$ = 116.3 (*N*Ph$_2$), 180.8 (*N*−Si(CH$_3$)$_2$*t*Bu), 205.2 ($^1J_{NH}$ = 65 Hz; *N*H), 289.8 ppm (L−*N*$_{py}$); $^1$H NMR (600 MHz, C$_6$D$_6$, 296 K) for **4b**: $\delta$ = 0.03, 0.42 (s, 6H; Si(C$H_3$)$_2$), 0.90 (s, 18H; Si−C(C$H_3$)$_3$), 0.95 (s, 3H; C$H_3$), 3.51 (d, $^2J_{HH}$ = 12.2 Hz, 2H; CH*H*), 4.09 (d, $^2J_{HH}$ = 12.2 Hz, 2H; C*H*H), 6.18 (s, 1H; N*H*), 6.32 (m, 1H; *H*5$_{py}$), 6.53 (m, 2H; *p*-*H*$_{Ph}$), 6.74 (d, $^3J_{H3pyH4py}$ = 8.0 Hz, 1H; *H*3$_{py}$), 6.94 (dt, $^3J_{H4pyH3py/H5py}$ = 7.7 Hz, $^4J_{H4pyH6py}$ = 1.3 Hz, 1H; *H*4$_{py}$), 7.17 (t, $^3J_{H5pyH6py}$ = 7.8 Hz, 4H; *m*-*H*$_{Ph}$), 7.40 (d, $^3J_{HoHm}$ = 8.1 Hz, 4H; *o*-*H*$_{Ph}$), 8.55 ppm (d, $^3J_{H6pyH5py}$ = 5.3 Hz, 1H; *H*6$_{py}$); $^{13}$C{$^1$H} NMR (100 MHz, C$_6$D$_6$, 296 K) for **4b**: $\delta$ = −4.0, −3.4 (Si−(C$H_3$)$_2$), 20.9 (Si−*C*(CH$_3$)$_3$), 28.0 (C−*C*H$_3$), 28.2 (Si−C(C$H_3$)$_3$), 48.2 (*C*−CH$_3$), 63.7 (C$H_2$), 120.8–123.1 (*m*-*C*$_{Ph}$, *p*-*C*$_{Ph}$, *C3*$_{py}$, *C5*$_{py}$, *o*-*C*$_{Ph}$), 139.9 (*C4*$_{py}$), 148.8 (*C6*$_{py}$), 150.8 (N−*C*$_{Ph}$), 162.1 ppm (*C2*$_{py}$); $^{29}$Si{$^1$H} NMR (80 MHz, C$_6$D$_6$, 296 K) for **4b**: $\delta$ = 3.16 ppm (*Si*(CH$_3$)$_2$*t*Bu); $^{15}$N NMR (60 MHz, C$_6$D$_6$, 296 K) for **4b**: $\delta$ = 103.5 (*N*Ph$_2$), 187.8 (*N*−Si(CH$_3$)$_2$*t*Bu), 207.9 ($^1J_{NH}$ = 66 Hz, *N*H), 281.7 ppm (L−*N*$_{py}$); IR (Nujol, NaCl) (mixture of the two isomers): $\tilde{\nu}$ = 3230 (w), 1603 (m), 1584 (s), 1486 (s), 1466 (s), 1378 (w), 1254 (m), 1141 (w), 1143 (w), 1059 (m), 1076 (m), 955 (w), 903 (s), 865 (s), 829 (m), 802 (m), 771 (m), 703 (w), 736 cm$^{-1}$ (w); elemental analysis for the mixture of the two isomers calcd (%) for C$_{20}$H$_{38}$N$_3$Si$_2$Cl$_2$Hf: C 50.24, H 6.64, N 8.88; found: C 50.22, H 6.81, N 8.92.

*Preparation of [Zr($N_2^{TBS}N_{py}$)(NNPh$_2$)(py)] (**5**)*: A solution of LiHMDS (548 mg, 4.15 mmol) in toluene (10 mL) was added dropwise over 5 min to a stirred solution of [Zr($N_2^{TBS}$N$_{py}$)(NHNPh$_2$)Cl] (2.30 g, 4.15 mmol) and pyridine (0.32 mL, 4.15 mmol) in toluene (50 mL). The reaction mixture was stirred overnight before the precipitated LiCl was removed by filtration and the volatiles were removed under reduced pressure. The resulting brown solid was washed with pentane (3×20 mL) before drying under vacuum to yield [Zr($N_2^{TBS}$N$_{py}$)(NNPh$_2$)(py)] as a dark green solid (1.77 g, 73 %). Single crystals for X-ray diffraction were grown from a saturated solution in toluene at 10 °C. $^1$H NMR (400 MHz, C$_6$D$_6$, 296 K): $\delta$ = −0.11, 0.06 (s, 6H; Si(C$H_3$)$_2$), 0.79 (s, 18H; Si−C(C$H_3$)$_3$), 1.15 (s, 3H; C$H_3$), 3.53 (d, $^2J_{HH}$ = 12.6 Hz, 2H; CH*H*), 3.98 (d, $^2J_{HH}$ = 12.5 Hz, 2H; C*H*H), 6.46 (ddd, $^3J_{H5pyH4py}$ = 7.5 Hz, $^3J_{H5pyH6py}$ = 5.3 Hz, $^4J_{H5pyH3py}$ = 1.0 Hz, 1H; *H*5$_{py}$), 6.54 (ddd, $^3J_{mHpypHpy}$ = 7.6 Hz, $^3J_{mHpyoHpy}$ = 4.9 Hz, $^5J_{mHpyoHpy}$ = 1.3 Hz, 2H; *m*-*H*$_{py}$), 6.82 (tt, $^3J_{pHmH}$ = 7.7 Hz, $^4J_{pHoH}$ = 1.5 Hz, 1H; *p*-*H*$_{py}$), 6.85–6.90 (sh, 3H; *p*-*H*$_{Ph}$, *H*3$_{py}$), 7.04 (dt, $^3J_{H4pyH3py/5py}$ = 7.8 Hz, $^4J_{H4pyH6py}$ = 1.8 Hz, 1H; *H*4$_{py}$), 7.31 (tt, $^3J_{mHo/pH}$ = 8.6 Hz, $^5J_{mHoH}$ = 2.0 Hz, 4H; *m*-*H*$_{Ph}$), 7.87 (dd, $^3J_{oHmH}$ = 8.6 Hz, $^4J_{oHpH}$ = 1.1 Hz, 4H; *o*-*H*$_{Ph}$), 9.05 (dt, $^3J_{oHpymHpy}$ = 6.2 Hz, $^4J_{oHpypHpy}$ = 1.5 Hz, 2H; *o*-*H*$_{py}$), 9.63 ppm (dd, $^3J_{H6pyH5py}$ = 5.3 Hz, $^4J_{H6pyH4py}$ = 1.1 Hz, 1H; *H6*$_{py}$); $^{13}$C{$^1$H} NMR (100 MHz, C$_6$D$_6$, 296 K): $\delta$ = −3.2 (Si(C$H_3$)$_2$), 20.5 (C−CH$_3$), 25.7 (Si−*C*(CH$_3$)$_3$), 27.9 (Si−C(C$H_3$)$_3$), 47.3 (*C*−CH$_3$), 64.2 (C$H_2$), 119.5 (*o*-*C*$_{Ph}$), 120.0 (*p*-C$_{Ph}$, *C3*$_{py}$), 121.1 (*C5*$_{py}$), 123.9 (*m*-*C*$_{py}$), 128.9 (*m*-C$_{Ph}$), 138.5 (*p*-C$_{py}$), 138.6 (*C4*$_{py}$), 149.3 (*C6*$_{py}$, *p*-*C*$_{py}$), 152.3 (N−*C*$_{Ph}$), 161.5 ppm (*C2*$_{py}$); $^{29}$Si{$^1$H} NMR (80 MHz, C$_6$D$_6$, 296 K): $\delta$ = 0.2 ppm (*Si*(CH$_3$)$_2$*t*Bu); $^{15}$N NMR (60 MHz, C$_6$D$_6$, 296 K): $\delta$ = 142.1 (*N*−Si(CH$_3$)$_2$*t*Bu), 178.2 (*N*Ph$_2$), 280.6 (*N*$_{py}$), 287.8 (ZrN), 291.4 ppm (L−*N*$_{py}$); IR (Nujol, NaCl): $\tilde{\nu}$ = 1597 (w), 1464 (m), 1273 (w), 1153 (w), 1062 (w), 894 (w), 870 (w), 742 (w), 694 cm$^{-1}$ (w); elemental analysis calcd (%) for C$_{38}$H$_{56}$N$_6$Si$_2$Zr: C 61.32, H 7.58, N 11.29; found: C 60.92, H 7.47, N 11.16.

*Preparation of [Hf($N_2^{TBS}N_{py}$)(NNPh$_2$)(py)] (**6**)*: A Schlenk tube was charged with [Hf($N_2^{TBS}$N$_{py}$)(NHNPh$_2$)Cl] (0.70 g, 0.9 mmol), pyridine (72 μL, 0.9 mmol) and toluene (10 mL). The mixture was stirred and a solution of LiHMDS (0.15 mg, 0.9 mmol) in toluene (2 mL) was added dropwise over 5 min. The reaction mixture was stirred for two days at room temperature. The precipitated LiCl was removed by filtration and the volatiles were removed under reduced pressure. The crude product was washed with pentane (3×5 mL) and dried under vacuum to yield a dark green solid (0.51 g, 0.6 mmol, 67 %). $^1$H NMR (600 MHz, C$_6$D$_6$, 296 K): $\delta$ = −0.12, 0.06 (s, 6H; Si(C$H_3$)$_2$), 0.78 (s, 18H; Si−C(C$H_3$)$_3$), 1.11 (s, 3H; C$H_3$), 3.60 (d, $^2J_{HH}$ = 12.4 Hz, 2H; CH*H*), 3.99 (d, $^2J_{HH}$ = 12.4 Hz, 2H; C*H*H), 6.43 (dd, $^3J_{H5pyH4py}$ = 7.4 Hz, $^4J_{H5pyH3py}$ = 1.0 Hz, 1H; *H*5$_{py}$), 6.52 (dd, $^3J_{mHpypHpy}$ = 7.5 Hz, $^4J_{mHpyoHpy}$ = 1.3 Hz, 2H; *m*-*H*$_{py}$), 6.80 (tt, $^3J_{pHmH}$ = 7.7 Hz, $^4J_{pHoH}$ = 1.7 Hz, 1H; *p*-*H*$_{py}$), 6.84 (d, $^3J_{H3pyH4py}$ = 8.2 Hz, 1H; *H*3$_{py}$), 6.86 (t, $^3J_{pHmH}$ = 7.2 Hz, 2H; *p*-*H*$_{Ph}$), 7.02 (dt, $^3J_{H4pyH3py/H5py}$ = 7.9 Hz, $^4J_{H4pyH6py}$ = 1.8 Hz, 1H; *H*4$_{py}$), 7.33 (t, $^3J_{mHo/pH}$ = 7.8 Hz, 4H; *m*-*H*$_{Ph}$), 7.93 (d, $^3J_{oHmH}$ = 7.8 Hz, 4H; *o*-*H*$_{Ph}$), 9.11 (m, 2H; *o*-*H*$_{py}$), 9.73 ppm (dd, $^3J_{H6pyH5py}$ = 5.2 Hz, $^4J_{H6pyH4py}$ = 1.1 Hz, 1H; *H6*$_{py}$); $^{13}$C{$^1$H} NMR (100 MHz, C$_6$D$_6$, 296 K): $\delta$ = −3.2 (Si(C$H_3$)$_2$), 20.6 (C−CH$_3$), 25.4 (Si−*C*-(CH$_3$)$_3$), 27.9 (Si−C(C$H_3$)$_3$), 46.3 (*C*−CH$_3$), 64.2 (C$H_2$), 119.4, 119.6 (*o*-

  

$C_{Ph}$, *p*-$C_{Ph}$), 120.2 (*C*3$_{py}$), 121.5 (*C*5$_{py}$), 124.0 (*m*-$C_{py}$), 128.8 (*m*-$C_{Ph}$), 138.7 (*p*-$C_{py}$, *C4*), 149.5 (N–$C_{Ph}$), 152.3 (*C*6$_{py}$, *o*-$C_{py}$), 161.4 ppm (*C*2$_{py}$); $^{29}$Si{$^1$H} NMR (80 MHz, $C_6D_6$, 296 K): $\delta = 2.16$ ppm (*Si*(CH$_3$)$_2$*t*Bu); $^{15}$N NMR (60 MHz, $C_6D_6$, 296 K): $\delta = 137.5$ (*N*–Si(CH$_3$)$_2$*t*Bu), 173.6 (*N*Ph$_2$), 281.7 (*N*$_{py}$), 281.7 (*N*$_{py}$), 285.1 (Hf*N*), 289.1 ppm (L–*N*$_{py}$); IR (Nujol, NaCl): $\tilde{\nu}$ = 2362 (w), 2343 (w), 1581 (sh), 1463 (s), 1377 (sh), 1296 (w), 1273 (m), 1257 (sh), 1163 (w), 1086 (w), 1076 (m), 898 (m), 876 (s), 805 (m), 694 cm$^{-1}$ (w); elemental analyses of **6** were systematically too low in carbon, which we attribute to carbide formation.

*Preparation of [Zr(N$_2^{TBS}$N$_{py}$)(NNPh$_2$){B(C$_6$F$_5$)$_3$}] (**7**)*: A solution of B(C$_6$F$_5$)$_3$ (174 mg, 0.34 mmol, 2 equiv) in toluene (2 mL) was added to a solution of [Zr(N$_2^{TBS}$N$_{py}$)(NNPh$_2$)(py)] (**3**) (126 mg, 0.17 mmol) in toluene (4 mL). The dark green solution was concentrated and colourless crystals were obtained after two days at RT (90 mg, 0.08 mmol, 47 %). $^1$H NMR (400 MHz, [D$_8$]THF, 296 K): $\delta = -0.01$, 0.23 (s, 6H; Si(C*H*$_3$)$_2$), 0.83 (s, 18H; Si–C(C*H*$_3$)$_3$), 1.66 (s, 3H; C*H*$_3$), 3.50 (d, $^2J_{HH} = 12.3$ Hz, 2H; CH*H*), 4.02 (d, $^2J_{HH} = 12.3$ Hz, 2H; C*H*H), 7.06 (m, 6H; *m*/*p*-*H*$_{Ph}$), 7.19 (m, 1H; *H5*$_{py}$), 7.32 (m, 4H; *o*-*H*$_{Ph}$), 7.79 (d, $^3J_{H3py/H4py} = 8.1$ Hz, 1H; *H3*$_{py}$), 8.07 (m, 1H; *H4*$_{py}$), 8.55 ppm (d, $^3J_{H3py/H4py} = 5.5$ Hz, 1H; *H6*$_{py}$); $^{13}$C{$^1$H} NMR (100 MHz, [D$_8$]THF, 296 K): $\delta = -4.0$, $-3.6$ (Si(*C*H$_3$)$_2$), 25.7 (C–*C*H$_3$, Si–*C*(CH$_3$)$_3$), 27.5 (Si–C(*C*H$_3$)$_3$), 48.9 (*C*–CH$_3$), 62.0 (*C*H$_2$), 121.9 (*C*3$_{py}$), 122.3 (*C*5$_{py}$), 128.0 (*o*/*m*/*p*-*C*$_{Ph}$), 137.2 (N–*C*$_{Ph}$), 142.7 (*C*4$_{py}$), 148.9 (*C*6$_{py}$), 163.0 ppm (*C*2$_{py}$); $^{29}$Si{$^1$H} NMR (80 MHz, [D$_8$]THF, 296 K): $\delta = 7.4$ ppm (*Si*(CH$_3$)$_2$*t*Bu); $^{11}$B NMR (65 MHz, [D$_8$]THF, 296 K): $\delta = -8.6$ ppm (N*B*(C$_6$F$_5$)$_3$); $^{19}$F NMR (380 MHz, [D$_8$]THF, 296 K): $\delta = -167.7$ (m), $-163.0$ (m), $-149.6$ (brs), $-131.0$ (brs), $-121.8$ ppm (brs; (BC$_6$*F*$_5$)$_3$); $^{15}$N NMR (60 MHz, [D$_8$]THF, 296 K): $\delta = 109.3$ (*N*Ph$_2$), 192.0 (*N*–Si(CH$_3$)$_2$*t*Bu), 266.2 ppm (*N*$_{py}$); the resonance of Zr–*N* was not observed; elemental analysis calcd (%) for $C_{51}H_{51}BF_{15}N_5Si_2Zr$: C 52.04, H 4.37, N 5.95; found: C 52.12, H 4.41, N 6.07.

*Preparation of [Hf(N$_2^{TBS}$N$_{py}$)(NNPh$_2$){B(C$_6$F$_5$)$_3$}] (**8**)*: B(C$_6$F$_5$)$_3$ (165 mg, 0.32 mmol, 2 equiv) in toluene (1 mL) was added to a solution of [Hf(N$_2^{TBS}$N$_{py}$)(NNPh$_2$)(py)] (134 mg, 0.16 mmol) in toluene (2 mL). The mixture immediately turned red. The solution was concentrated and stored at 10 °C. After two days colourless crystals precipitated. The product was separated from the mother liquor by filtration and washed with toluene. Yield: 100 mg (0.08 mmol, 50 %). $^1$H NMR (400 MHz, [D$_8$]THF, 333 K): $\delta = 0.00$, 0.24 (s, 6H; Si(C*H*$_3$)$_2$), 0.85 (s, 18H; Si–C(C*H*$_3$)$_3$), 1.61 (s, 3H; C*H*$_3$), 3.67 (d, $^2J_{HH} = 12.4$ Hz, 2H; CH*H*), 4.16 (d, $^2J_{HH} = 12.4$ Hz, 2H; C*H*H), 7.02–7.13 (m, 5H; *m*-*H*$_{Ph}$, *H5*$_{py}$), 7.16 (d, $^3J_{pHmH} = 7.4$ Hz, 2H; *o*-*H*$_{Ph}$), 7.38 (m, 4H; *p*-*H*$_{Ph}$), 7.77 (d, $^3J_{H3py/H4py} = 8.0$ Hz, 1H; *H3*$_{py}$), 8.06 (d, $^3J_{H4pyH5py/H3py} = 7.6$ Hz, 1H; *H4*), 8.60 ppm (d, $^3J_{H6pyH5py} = 5.4$ Hz, 1H; *H6*$_{py}$); $^{13}$C{$^1$H} NMR (100 MHz, $C_6D_6$, 296 K): $\delta = -2.8$, $-2.5$ (Si(*C*H$_3$)$_2$), 20.9 (Si–*C*(CH$_3$)$_3$), 25.8 (C–*C*H$_3$), 28.6 (Si–C(*C*H$_3$)$_3$), 48.5 (*C*–CH$_3$), 62.4 (*C*H$_2$), 123.3 (*C*3$_{py}$), 123.9 (C5$_{py}$), 128.8 (*o*-*C*$_{Ph}$, *m*-*C*$_{Ph}$, *p*-*C*$_{Ph}$), 138.5 (N–*C*$_{Ph}$), 144.2 (*C*6$_{py}$), 150.0 ppm (*C*2$_{py}$); $^{29}$Si{$^1$H} NMR (80 MHz, [D$_8$]THF, 296 K): $\delta = 9.11$ ppm (*Si*(CH$_3$)$_2$*t*Bu); $^{15}$N NMR (60 MHz, [D$_8$]THF, 296 K): $\delta = 111.6$ (*N*Ph$_2$), 177.2 (*N*–Si(CH$_3$)$_2$*t*Bu), 269.1 ppm (L–*N*$_{py}$), not observed (Hf*N*); IR (Nujol, NaCl): $\tilde{\nu}$ = 1646 (m), 1610 (w), 1519 (m), 1463 (s), 1377 (s), 1261 (m), 1090 (sh), 1019 (sh), 873 (sh), 801 (m), 723 cm$^{-1}$ (w); elemental analysis calcd (%) for $C_{51}H_{51}N_5BF_{15}Si_2Hf$: C 48.44, H 4.07, N 5.54; found: C 48.76, H 4.31, N 5.42.

*Thermal rearrangement of **7** to [Zr(N$_2^{TBS}$N$_{py}$)(C$_6$F$_5$)(κ-N′}Ph$_2$NN′{B(C$_6$F$_5$)$_2$}] (**9**)*: A solution of **7** in [D$_8$]toluene (0.5 mL) was heated to 65 °C for 48 h. The colourless solution turned yellow. The rearrangement product was characterised by NMR spectroscopy. $^1$H NMR (600 MHz, $C_7D_8$, 330 K): $\delta = -0.83$, 0.05 (s, 6H; Si(C*H*$_3$)$_2$), 0.63 (s, 18H; Si–C(C*H*$_3$)$_3$), 0.95 (s, 3H; C*H*$_3$), 3.03 (d, $^2J_{HH} = 12.9$ Hz, 2H; CH*H*), 3.35 (brs, 2H; C*H*H), 6.59 (m, 1H; *H5*$_{py}$), 6.82 (m, 2H; *p*-*H*$_{Ph}$), 6.80 (m, 1H; *H3*$_{py}$), 7.05 (m, 1H; *H4*$_{py}$), 7.08 (m, 4H; *m*-*H*$_{Ph}$), 7.65 (d, $^3J_{oH/mH} = 8.0$ Hz, 4H; *o*-*H*$_{Ph}$), 8.77 ppm (d, $^3J_{H6py/H5py} = 5.6$ Hz, 1H; *H6*$_{py}$); $^{13}$C{$^1$H} NMR (150.9 MHz, $C_7D_8$, 330 K): $\delta = -6.5$, $-4.7$ (Si(*C*H$_3$)$_2$), 20.1 (C–*C*H$_3$), 20.4 (Si–*C*(CH$_3$)$_3$), 27.0 (Si–C(*C*H$_3$)$_3$), 48.4 (*C*–CH$_3$), 63.1 (*C*H$_2$), 119.8 (*C*3$_{py}$), 121.6 (*C*5$_{py}$), 122.9 (*o*-*C*$_{Ph}$), 128.2 (*m*/*p*-*C*$_{Ph}$), 138.2 (*C*4$_{py}$), 145.3 (*C*6$_{py}$), 147.8 (N–*C*$_{Ph}$), 159.7 ppm (*C*2$_{py}$), not observed (*C*$_{ArF}$); $^{29}$Si{$^1$H} NMR (79.4 MHz, $C_7D_8$, 295 K): $\delta = 2.4$ ppm (*Si*(CH$_3$)$_2$*t*Bu); $^{15}$N NMR (60 MHz, [D$_8$]toluene, 295 K): $\delta = 119.3$ (*N*Ph$_2$), 148.6 (*N*–Si(CH$_3$)$_2$*t*Bu), 280.6 ppm (*N*$_{py}$), not observed (Zr–*N*); $^{11}$B NMR (128.3 MHz, $C_7D_8$, 295 K): $\delta$ = 38.4 ppm (N*B*(C$_6$F$_5$)$_2$).

Table 6. Details of the crystal structure determinations of **3a**, **5**, **7** and **8**.

| | **3a** | **5** | **7** | **8** |
|---|---|---|---|---|
| formula | $C_{33}H_{52}ClN_5Si_2Zr$ | $C_{38}H_{56}N_6Si_2Zr$ | $C_{51}H_{51}BF_{15}N_5Si_2Zr$ | $C_{51}H_{51}BF_{15}HfN_5Si_2{\cdot}C_7H_8$ |
| crystal system | orthorhombic | monoclinic | monoclinic | triclinic |
| space group | *Pna*2$_1$ | *P*2$_1$/*c* | *P*2$_1$/*c* | *P*$\bar{1}$ |
| *a* [Å] | 10.2241(15) | 10.2312(9) | 23.0267(13) | 12.060(1) |
| *b* [Å] | 35.855(5) | 12.4990(11) | 10.7753(6) | 12.778(1) |
| *c* [Å] | 9.8844(15) | 30.880(3) | 20.6324(12) | 20.345(2) |
| $\alpha$ [°] | – | – | – | 100.548(2) |
| $\beta$ [°] | – | 97.632(2) | 97.988(1) | 92.719(2) |
| $\gamma$ [°] | – | – | – | 109.121(2) |
| *V* [Å$^3$] | 3623.5(9) | 3913.9(6) | 5069.6(5) | 2892.8(5) |
| *Z* | 4 | 4 | 4 | 2 |
| $M_r$ | 701.65 | 744.29 | 1177.18 | 1356.58 |
| $\rho_{calcd}$ [g cm$^{-3}$] | 1.286 | 1.263 | 1.542 | 1.557 |
| $F_{000}$ | 1480 | 1576 | 2400 | 1364 |
| $\mu$ (Mo$_{K\alpha}$) [mm$^{-1}$] | 0.472 | 0.38 | 0.362 | 1.936 |
| max., min. transmission factors | 0.7451, 0.5869 | 0.7459, 0.6030 | 0.7464, 0.6860 | 0.4346, 0.3659 |
| data collection *T* [K] | 150(2) | 150(2) | 100(2) | 100(2) |
| $\theta$ range [°] | 2.1 to 25.0 | 2.0 to 28.5 | 2.0 to 29.6 | 2.0 to 32.2 |
| *h*,*k*,*l* (independent set) | 0 to 12, 0 to 42, −11 to 11 | −13 to 13, −16 to 0, −40 to 12 | −31 to 31, 0 to 14, −28 to 0 | −18 to 17, −19 to 18, 0 to 30 |
| reflections measured | 55914 | 75589 | 117097 | 72399 |
| unique reflections [$R_{int}$] | 6390 [0.1609] | 8978 [0.0983] | 14210 [0.0905] | 19035 [0.0341] |
| reflections obsd [$I = 2\sigma(I)$] | 4356 | 6203 | 9711 | 16690 |
| parameters refined | 390 | 435 | 687 | 814 |
| $R(F)$, $wR(F^2)$ [$F > 4\sigma(F)$] | 0.0628, 0.1366 | 0.0485, 0.1113 | 0.0457, 0.1065 | 0.0276, 0.0633 |
| $R(F)$, $wR(F^2)$ (all data) | 0.0932, 0.1525 | 0.0789, 0.1236 | 0.0746, 0.1173 | 0.0390, 0.0707 |
| GooF on $F^2$ | 0.93 | 1.03 | 1.09 | 1.11 |
| absolute structure parameter | −0.08(7) | – | – | – |
| largest residual peaks [e Å$^{-3}$] | 0.431, −0.725 | 0.561, −0.773 | 1.208, −0.633 | 1.818, −0.983 |

**Crystal structure determinations**: Crystal data and details of the structure determinations are listed in Table 6. Intensity data were collected at low temperature with a Bruker AXS Smart 1000 CCD diffractometer ($Mo_{K\alpha}$ radiation, graphite monochromator, $\lambda = 0.71073$ Å). Data were corrected for Lorentz, polarisation and absorption effects (semiempirical, SADABS).[25] The structures were solved by the heavy-atom method combined with structure expansion by using direct methods applied to difference structure factors[26] or by using direct methods with dual-space recycling ("Shake-and-Bake")[27] and refined by means of full-matrix least-squares methods based on $F^2$ against all reflections.[28] All non-hydrogen atoms were given anisotropic displacement parameters. Hydrogen atoms (except that on N(4) of **3a**, the position of which was taken from a difference Fourier synthesis) were placed in calculated positions and refined with a riding model. Disordered solvent of crystallisation (toluene) in the structure of **8** was subjected to planarity and appropriate distance restraints.

CCDC-686263 (**3a**), 658106 (**5**), 686264 (**7**) and 686265 (**8**) contain the supplementary crystallographic data for this paper. These data can be obtained free of charge from The Cambridge Crystallographic Data Centre via www.ccdc.cam.ac.uk/data_request/cif.

**Computational studies**: All the calculations have been made with the Gaussian 03 program.[29] DFT calculations with the non-local hybrid B3PW91 functional[14] and Stuttgart relativistic, small core ECP basis set for the Zr atom and the 6-31G(d) basis set for rest of the atoms were performed.[30] Better geometrical parameters were obtained with the introduction of a polarisation function to the Zr atom. This approach is widely used for computational studies of transition-metal complexes yielding consistent results. Electronic structures were studied by using natural bond orbital (NBO) analysis,[17,31] with the NBO 3.0 facilities built into Gaussian 03. In particular, linear natural molecular orbitals (NLMO) ("delocalisation tails")[15] and natural population analysis (NPA) (partial charge distribution) were used.[17] As a semi-quantitative measure of the bond order, the Wiberg bond index was used.[23] All the orbital visualisations have been obtained with the GaussView[32] and Molekel[33] programs. The molecular systems studied were optimised starting from X-ray diffraction data. Following geometry optimisation, frequency calculations were performed on all calculated structures to ensure that there were no imaginary frequencies.

## Acknowledgements

We thank the Deutsche Forschungsgemeinschaft for funding and the MEC (Spain) for a postdoctoral fellowship (to J.L.F.).

[1] Examples of titanium hydrazinediides: a) N. Wiberg, H.-W. Haring, G. Huttner, P. Friedrich, *Chem. Ber.* **1978**, *111*, 2708; b) A. J. Blake, J. M. McInnes, P. Mountford, G. I. Nikonov, D. Swallow, D. J. Watkin, *J. Chem. Soc. Dalton Trans.* **1999**, 379; c) J. L. Thormann, L. K. Woo, *Inorg. Chem.* **2000**, *39*, 1301; d) Y. Li, Y. Shi, A. L. Odom, *J. Am. Chem. Soc.* **2004**, *126*, 1794; e) T. B. Parsons, N. Hazari, A. R. Cowley, J. C. Green, P. Mountford, *Inorg. Chem.* **2005**, *44*, 8442; f) S. Patel, Y. Li, A. L. Odom, *Inorg. Chem.* **2007**, *46*, 6373; g) J. D. Selby, C. D. Manley, M. Feliz, A. D. Schwarz, E. Clot, P. Mountford, *Chem. Commun.* **2007**, 4937; selected examples of hydrazido(1−) titanium complexes: h) I. A. Latham, G. J. Leigh, G. Huttner, I. Jibril, *J. Chem. Soc. Dalton Trans.* **1986**, 385; i) D. L. Hughes, M. Jimenez-Tenorio, G. J. Leigh, D. G. Walker, *J. Chem. Soc. Dalton Trans.* **1989**, 2389; j) S.-J. Kim, I. N. Jung, B. R. Yoo, S. Cho, J. Ko, S. H. Kim, S. O. Kang, *Organometallics* **2001**, *20*, 1501; k) S. C. Yoon, B. A. Bae, I.-H. Sub, J. T. Park, *Organometallics* **1999**, *18*, 2049; l) T. Zippel, P. Amdt, A. Ohff, A. Spannenberg, R. Kempe, U. Rosenthal, *Organometallics* **1998**, *17*, 4429; m) J. E. Hill, P. E. Fanwick, I. P. Rothwell, *Inorg. Chem.* **1991**, *30*, 1143; n) B. Goetze, J. Knizek, H. Nöth, W. Schnick, *Eur. J. Inorg. Chem.* **2000**, 1849.

[2] a) J. S. Johnson, R. G. Bergmann, *J. Am. Chem. Soc.* **2001**, *123*, 2923; b) C. Cao, Y. Shi, A. L. Odom, *Org. Lett.* **2002**, *4*, 2853; c) V. Khedkar, A. Tillack, M. Michalik, M. Beller, *Tetrahedron Lett.* **2004**, *45*, 3123; d) L. Ackermann, R. Born, *Tetrahedron Lett.* **2004**, *45*, 9541.

[3] a) S. Banerjee, Y. Shi, C. Cao, A. L. Odom, *J. Organomet. Chem.* **2005**, *690*, 5066; b) S. Banerjee, A. L. Odom, *Organometallics* **2006**, *25*, 3099.

[4] A. Tillack, H. Jiao, I. Garcia Castro, C. G. Hartung, M. Beller, *Chem. Eur. J.* **2004**, *10*, 2410.

[5] a) P. J. Walsh, M. J. Carney, R. G. Bergman, *J. Am. Chem. Soc.* **1991**, *113*, 6343; for a very recent overview of the N−N reactivity of hydrazides and related complexes, see: b) D. J. Mindiola, *Angew. Chem.* **2008**, *120*, 1580; *Angew. Chem. Int. Ed.* **2008**, *47*, 1557.

[6] a) S. Friedrich, M. Schubart, L. H. Gade, I. J. Scowen, A. J. Edwards, M. McPartlin, *Chem. Ber.* **1997**, *130*, 1751; review: b) L. H. Gade, *Chem. Commun.* **2000**, 173.

[7] a) A. J. Blake, P. E. Collier, L. H. Gade, M. McPartlin, P. Mountford, M. Schubart, I. J. Scowen, *Chem. Commun.* **1997**, 1555; b) A. J. Blake, P. E. Collier, L. H. Gade, P. Mountford, S. E. Pugh, M. Schubart, D. J. M. Trösch, *Inorg. Chem.* **2001**, *40*, 870; c) B. D. Ward, A. Maisse-François, P. Mountford, L. H. Gade, *Chem. Commun.* **2004**, 704; review: d) L. H. Gade, P. Mountford, *Coord. Chem. Rev.* **2001**, *216/217*, 65.

[8] H. Herrmann, J. Lloret Fillol, H. Wadepohl, L. H. Gade, *Angew. Chem.* **2007**, *119*, 8578; *Angew. Chem. Int. Ed.* **2007**, *46*, 8426.

[9] Theoretical analysis of the bonding of hydrazido ligands: a) S. Kahlal, J. Saillard, J. Hamon, C. Manzur, D. Carrillo, *J. Chem. Soc. Dalton Trans.* **1998**, 1229; b) S. Kahlal, J. Saillard, J. Hamon, C. Manzur, D. Carrillo, *New J. Chem.* **2001**, *25*, 231.

[10] H. Herrmann, H. Wadepohl, L. H. Gade, *Dalton Trans.* **2008**, 2111.

[11] X.-R. Sun, J.-S. Huang, K.-K. Cheung, C.-M. Che, *Inorg. Chem.* **2000**, *39*, 820.

[12] C. Bustos, C. Manzur, D. Carrillo, F. Robert, P. Gouzerh, *Inorg. Chem.* **1994**, *33*, 1427.

[13] H. Herrmann, J. Lloret Fillol, H. Wadepohl, L. H. Gade, *Organometallics* **2008**, *27*, 172.

[14] a) A. D. Becke, *J. Chem. Phys.* **1993**, *98*, 5648; b) J. P. Perdew, Y. Wang, *Phys. Rev. B* **1992**, *45*, 13244.

[15] a) A. E. Reed, F. Weinhold, *J. Chem. Phys.* **1985**, *83*, 1736; b) A. E. Reed, R. B. Weinstock, F. Weinhold, *J. Chem. Phys.* **1985**, *83*, 735.

[16] N. Vujkovic, B. D. Ward, A. Maisse-François, H. Wadepohl, P. Mountford, L. H. Gade, *Organometallics* **2007**, *26*, 5522.

[17] a) J. E. Carpenter, F. Weinhold, *THEOCHEM* **1988**, *169*, 41; b) J. E. Carpenter, Ph.D. thesis, University of Wisconsin, Madison, WI (USA), **1987**; c) J. P. Foster, F. Weinhold, *J. Am. Chem. Soc.* **1980**, *102*, 7211.

[18] a) T. E. Glassman, M. G. Vale, R. R. Schrock, *J. Am. Chem. Soc.* **1992**, *114*, 8098; b) P. S. Wagenknecht, J. R. Norton, *J. Am. Chem. Soc.* **1995**, *117*, 1841.

[19] H. Nöth, B. Wrackmeyer, *Nuclear Magnetic Resonance Spectroscopy of Boron Compounds*, Springer, Berlin, Heidelberg, New York, **1978**, p. 169.

[20] M. A. Bush, G. A. Sinn, *J. Chem. Soc. A* **1971**, 2225.

[21] A. Bondi, *J. Phys. Chem.* **1964**, *68*, 441.

[22] a) N. Kleigrewe, T. Brackemeyer, G. Kehr, R. Fröhlich, G. Erker, *Organometallics* **2001**, *20*, 1952; for other examples of betaine-type complexes of group 4 metals containg a $B(C_6F_5)_3$ unit, see: b) J. Ruwwe, G. Erker, R. Fröhlich, *Angew. Chem.* **1996**, *108*, 108; *Angew. Chem. Int. Ed. Engl.* **1996**, *35*, 80; c) P. Arndt, W. Baumann, A. Spannenberg, U. Rosenthal, V. V. Burkalov, V. B. Shur, *Angew. Chem.* **2003**, *115*, 1455; *Angew. Chem. Int. Ed.* **2003**, *42*, 1414; d) F. Hannig, R. Fröhlich, K. Bergander, G. Erker, J. L. Petersen, *Organometallics* **2004**, *23*, 4495.

[23] K. B. Wiberg, *Tetrahedron* **1968**, *24*, 1083.

[24] a) T. Wondimagegn, Z. Xu, K. Vanka, T. Ziegler, *Organometallics* **2004**, *23*, 3847; b) X. Yang, C. L. Stern, T. J. Marks, *J. Am. Chem. Soc.* **1994**, *116*, 10015.

[25] G. M. Sheldrick, SADABS, Bruker AXS, **2004–2008**.

  

[26] P. T. Beurskens in *Crystallographic Computing 3* (Eds.: G. M. Sheldrick, C. Krüger, R. Goddard), Clarendon Press, Oxford (UK), **1985**, p. 216; P. T. Beurskens, G. Beurskens, R. de Gelder, J. M. M. Smits, S. Garcia-Granda, R. O. Gould, DIRDIF-2008, Raboud University, Nijmegen (The Netherlands), **2008**.

[27] M. C. Burla, R. Caliandro, M. Camalli, B. Carrozzini, G. L. Cascarano, L. De Caro, C. Giacovazzo, G. Polidori, R. Spagna, SIR2004, CNR IC, Bari (Italy), **2004**; M. C. Burla, R. Caliandro, M. Camalli, B. Carrozzini, G. L. Cascarano, L. De Caro, C. Giacovazzo, G. Polidori, R. Spagna, *J. Appl. Crystallogr.* **2005**, *38*, 381.

[28] G. M. Sheldrick, SHELXS-97, University of Göttingen, **1997**; G. M. Sheldrick, *Acta Crystallogr. Sect. A* **2008**, *64*, 112.

[29] Gaussian 03 (Revision D.02), M. J. Frisch, G. W. Trucks, H. B. Schlegel, G. E. Scuseria, M. A. Robb, J. R. Cheeseman, J. A. Montgomery, Jr., T. Vreven, K. N. Kudin, J. C. Burant, J. M. Millam, S. S. Iyengar, J. Tomasi, V. Barone, B. Mennucci, M. Cossi, G. Scalmani, N. Rega, G. A. Petersson, H. Nakatsuji, M. Hada, M. Ehara, K. Toyota, R. Fukuda, J. Hasegawa, M. Ishida, T. Nakajima, Y. Honda, O. Kitao, H. Nakai, M. Klene, X. Li, J. E. Knox, H. P. Hratchian, J. B. Cross, V. Bakken, C. Adamo, J. Jaramillo, R. Gomperts, R. E. Stratmann, O. Yazyev, A. J. Austin, R. Cammi, C. Pomelli, J. W. Ochterski, P. Y. Ayala, K. Morokuma, G. A. Voth, P. Salvador, J. J. Dannenberg, V. G. Zakrzewski, S. Dapprich, A. D. Daniels, M. C. Strain, O. Farkas, D. K. Malick, A. D. Rabuck, K. Raghavachari, J. B. Foresman, J. V. Ortiz, Q. Cui, A. G. Baboul, S. Clifford, J. Cioslowski, B. B. Stefanov, G. Liu, A. Liashenko, P. Piskorz, I. Komaromi, R. L. Martin, D. J. Fox, T. Keith, M. A. Al-Laham, C. Y. Peng, A. Nanayakkara, M. Challacombe, P. M. W. Gill, B. Johnson, W. Chen, M. W. Wong, C. Gonzalez, J. A. Pople, Gaussian, Inc., Wallingford CT, **2004**.

[30] a) W. J. Hehre, R. Ditchfield, J. A. Pople, *J. Chem. Phys.* **1972**, *56*, 2257; b) P. C. Hariharan, J. A. Pople, *Theoret. Chim. Acta* **1973**, *28*, 213; c) M. M. Francl, W. J. Petro, W. J. Hehre, J. S. Binkley, M. S. Gordon, D. J. DeFress, J. A. Pople, *J. Chem. Phys.* **1982**, *77*, 3654; d) A. W. Ehlers, M. Bohme, S. Dapprich, A. Gobbi, A. Hollwarth, V. Jonas, K. F. Kohler, R. Stegmann, A. Veldkamp, G. Frenking, *Chem. Phys. Lett.* **1993**, *208*, 111; the basis set was obtained from the Extensible Computational Chemistry Environment Basis Set Database, version 9/12/01, as developed and distributed by the Molecular Science Computing Facility, Environmental and Molecular Sciences Laboratory, which is part of the Pacific Northwest Laboratory, P.O. Box 999, Richland, WA 99352 (US), and funded by the US Department of Energy.

[31] a) A. E. Reed, F. Weinhold, *J. Chem. Phys.* **1983**, *78*, 4066; b) A. E. Reed, L. A. Curtiss, F. Weinhold, *Chem. Rev.* **1988**, *88*, 899.

[32] R. Dennington, II, T. Keith, J. Millam, K. Eppinnett, W. L. Hovell, R. Gilliland, GaussView, Version 3.0, Semichem, Inc., Shawnee Mission, KS (USA), **2003**.

[33] P. Flükiger, H. P. Lüthi, H. Portmann, S. J. Weber, MOLEKEL 4.0, Swiss National Supercomputing Centre CSCS, Manno (Switzerland), **2000**.

Received: May 8, 2008
Published online: August 4, 2008

  